

International Journal of Physical Sciences

Volume 12 Number 23 16 December , 2017

ISSN 1992-1950



*Academic
Journals*

ABOUT IJPS

The **International Journal of Physical Sciences (IJPS)** is published weekly (one volume per year) by Academic Journals.

International Journal of Physical Sciences (IJPS) is an open access journal that publishes high-quality solicited and unsolicited articles, in English, in all Physics and chemistry including artificial intelligence, neural processing, nuclear and particle physics, geophysics, physics in medicine and biology, plasma physics, semiconductor science and technology, wireless and optical communications, materials science, energy and fuels, environmental science and technology, combinatorial chemistry, natural products, molecular therapeutics, geochemistry, cement and concrete research, metallurgy, crystallography and computer-aided materials design. All articles published in IJPS are peer-reviewed.

Contact Us

Editorial Office: ijps@academicjournals.org

Help Desk: helpdesk@academicjournals.org

Website: <http://www.academicjournals.org/journal/IJPS>

Submit manuscript online <http://ms.academicjournals.me/>

Editors

Prof. Sanjay Misra

*Department of Computer Engineering, School of Information and Communication Technology
Federal University of Technology, Minna,
Nigeria.*

Prof. Songjun Li

*School of Materials Science and Engineering,
Jiangsu University,
Zhenjiang,
China*

Dr. G. Suresh Kumar

*Senior Scientist and Head Biophysical Chemistry
Division Indian Institute of Chemical Biology
(IICB)(CSIR, Govt. of India),
Kolkata 700 032,
INDIA.*

Dr. Remi Adewumi Oluoyinka

*Senior Lecturer,
School of Computer Science
Westville Campus
University of KwaZulu-Natal
Private Bag X54001
Durban 4000
South Africa.*

Prof. Hyo Choi

*Graduate School
Gangneung-Wonju National University
Gangneung,
Gangwondo 210-702, Korea*

Prof. Kui Yu Zhang

*Laboratoire de Microscopies et d'Etude de
Nanostructures (LMEN)
Département de Physique, Université de Reims,
B.P. 1039. 51687,
Reims cedex,
France.*

Prof. R. Vittal

*Research Professor,
Department of Chemistry and Molecular
Engineering
Korea University, Seoul 136-701,
Korea.*

Prof Mohamed Bououdina

*Director of the Nanotechnology Centre
University of Bahrain
PO Box 32038,
Kingdom of Bahrain*

Prof. Geoffrey Mitchell

*School of Mathematics,
Meteorology and Physics
Centre for Advanced Microscopy
University of Reading Whiteknights,
Reading RG6 6AF
United Kingdom.*

Prof. Xiao-Li Yang

*School of Civil Engineering,
Central South University,
Hunan 410075,
China*

Dr. Sushil Kumar

*Geophysics Group,
Wadia Institute of Himalayan Geology,
P.B. No. 74 Dehra Dun - 248001(UC)
India.*

Prof. Suleyman KORKUT

*Duzce University
Faculty of Forestry
Department of Forest Industrial Engineering
Beciyorukler Campus 81620
Duzce-Turkey*

Prof. Nazmul Islam

*Department of Basic Sciences &
Humanities/Chemistry,
Techno Global-Balurghat, Mangalpur, Near District
Jail P.O: Beltalpark, P.S: Balurghat, Dist.: South
Dinajpur,
Pin: 733103,India.*

Prof. Dr. Ismail Musirin

*Centre for Electrical Power Engineering Studies
(CEPES), Faculty of Electrical Engineering, Universiti
Teknologi Mara,
40450 Shah Alam,
Selangor, Malaysia*

Prof. Mohamed A. Amr

*Nuclear Physic Department, Atomic Energy Authority
Cairo 13759,
Egypt.*

Dr. Armin Shams

*Artificial Intelligence Group,
Computer Science Department,
The University of Manchester.*

Editorial Board

Prof. Salah M. El-Sayed

*Mathematics. Department of Scientific Computing,
Faculty of Computers and Informatics,
Benha University. Benha ,
Egypt.*

Dr. Rowdra Ghatak

*Associate Professor
Electronics and Communication Engineering Dept.,
National Institute of Technology Durgapur
Durgapur West Bengal*

Prof. Fong-Gong Wu

*College of Planning and Design, National Cheng Kung
University
Taiwan*

Dr. Abha Mishra.

*Senior Research Specialist & Affiliated Faculty.
Thailand*

Dr. Madad Khan

*Head
Department of Mathematics
COMSATS University of Science and Technology
Abbottabad, Pakistan*

Prof. Yuan-Shyi Peter Chiu

*Department of Industrial Engineering & Management
Chaoyang University of Technology
Taichung, Taiwan*

Dr. M. R. Pahlavani,

*Head, Department of Nuclear physics,
Mazandaran University,
Babolsar-Iran*

Dr. Subir Das,

*Department of Applied Mathematics,
Institute of Technology, Banaras Hindu University,
Varanasi*

Dr. Anna Oleksy

*Department of Chemistry
University of Gothenburg
Gothenburg,
Sweden*

Prof. Gin-Rong Liu,

*Center for Space and Remote Sensing Research
National Central University, Chung-Li,
Taiwan 32001*

Prof. Mohammed H. T. Qari

*Department of Structural geology and remote sensing
Faculty of Earth Sciences
King Abdulaziz UniversityJeddah,
Saudi Arabia*

Dr. Jyhwen Wang,

*Department of Engineering Technology and Industrial
Distribution
Department of Mechanical Engineering
Texas A&M University
College Station,*

Prof. N. V. Sastry

*Department of Chemistry
Sardar Patel University
Vallabh Vidyanagar
Gujarat, India*

Dr. Edilson Ferneda

*Graduate Program on Knowledge Management and IT,
Catholic University of Brasilia,
Brazil*

Dr. F. H. Chang

*Department of Leisure, Recreation and Tourism
Management,
Tzu Hui Institute of Technology, Pingtung 926,
Taiwan (R.O.C.)*

Prof. Annapurna P.Patil,

*Department of Computer Science and Engineering,
M.S. Ramaiah Institute of Technology, Bangalore-54,
India.*

Dr. Ricardo Martinho

*Department of Informatics Engineering, School of
Technology and Management, Polytechnic Institute of
Leiria, Rua General Norton de Matos, Apartado 4133, 2411-
901 Leiria,
Portugal.*

Dr Driss Miloud

*University of mascara / Algeria
Laboratory of Sciences and Technology of Water
Faculty of Sciences and the Technology
Department of Science and Technology
Algeria*

Prof. Bidyut Saha,

*Chemistry Department, Burdwan University, WB,
India*

ARTICLES

- Microstructure and mechanical properties correlation for the steel:
A comparative methodology of educational research for physics
and mechanical engineering trainings** **322**
B. González-Vizcarra, F. Mesa, A. Delgado-Hernández, M. Avila-Puc,
J. M. Colores-Vargas, F. J. Ramírez-Arias M. Siqueiros-Hernández and
L. Cruz-Vazqu
- Intersection of lineaments for groundwater prospect analysis using
satellite remotely sensed and aeromagnetic dataset around Ibodi,
Southwestern Nigeria** **329**
Ilugbo S. O. and Adebisi A. D.

Full Length Research Paper

Microstructure and mechanical properties correlation for the steel: A comparative methodology of educational research for physics and mechanical engineering trainings

B. González-Vizcarra¹, F. Mesa^{1*}, A. Delgado-Hernández¹, M. Avila-Puc¹, J. M. Colores-Vargas¹, F. J. Ramírez-Arias¹, M. Siqueiros-Hernández¹ and L. Cruz-Vazquez²

¹School of Technology and Engineering Sciences, Autonomous University of Baja California, 21500 Tijuana, Baja California, Mexico.

²Department of Processes, Technological University of Tijuana (UTT). 22253 Tijuana, Baja California, México.

Received 7 September, 2017; Accepted 31 October, 2017

An academic methodology based for experimental evaluation of materials treatment is presented. The study is centered in an educational research emphasis about microstructure evaluation and heat treatments in steels samples machined according to ASTM E8 specifications. The uses of metallographic techniques and hardness/tensile tests for analyzing experimental variations due to structural changes are included. Different thermal treatments were applied on AISI-SAE 1018 steel specimens by raising the temperature until it reached the austenization state. Images were obtained with a Nikon NIS Elements computer programming, in order to observe the microstructure and identify the phases involved in each of the thermal treatments. For the hardness analysis, the round indenter of 1/16 in of Tungsten Carbide with a preload of 100 kg was used. A grain diameter of 3 to 4 μm was observed in both annealed and normalized sample, so it is assumed that the cold rolled or reference sample had a normalized condition. Both 41 and 67% in elongation and area reduction percentages, respectively, in the normalized samples were observed. The results allow identifying the correlation between microstructures and mechanical properties, providing an engineering educational approach for metallographic analysis and heat treatment schemes focused on the grain size interpretation, resilience and stress-strain curves. The described methodology provides an academic reference for the didactic evaluation of the main techniques associated with the treatment of materials for physics and mechanical engineering training.

Key words: Heat treatments, microstructure, tensile test, hardness, educational research.

INTRODUCTION

Since the beginning of civilization, materials have been used by humanity to improve their standard of living, being it the substances that make up any structure or product (Daunton et al., 2012; Whitesides and Wong, 2006). Engineers design most products and the

processes required for their manufacture are invoiced, so students of engineering must get acquainted with the internal structure and properties of the materials, as well as the techniques of thermal treatments, stress tests, hardness and metallographic analysis (Selfridge, 1985;

Williams and Starke, 2003; Parkinson, 1995). The engineer should be able to select the most suitable for each application and be able to develop the best processing methods.

Considering the role of the engineer training to meet such needs, important studies have been conducted to identify strategies and reflections that promote a more solid formation in the area of design (Atman et al., 2007; Schaefer et al., 2008; Szykman et al., 2000; Dym et al., 2005), as well as in the implementation of the scheme and learning project-based (Dutson et al., 1997; Mills and Tregust, 2003).

The thermal treatments constitute procedures to improve materials properties or achieve characteristics for specific purposes (Calik, 2009; Kuśtrowski et al., 2005; Fadare et al., 2011; Daramola et al., 2010; He et al., 2010) and these in turn, depend on the structure and the type of material in a piece, which is achieved with the precise handling of temperature and cooling rate. A recent study about the impact of intercritical annealing temperature and microstructure, including optical microscopy and point count method using stereology to evaluate martensite volume fraction, can be consulted in the report of Ikpeseni et al. (2015). Also, a description about the main heat treatment problems can be found in ASM Handbook, chapter 1 (ASM Handbook, 2014).

Other properties associated with the materials, such as the structural characteristics and its relation to the physical, mechanical and chemical properties are usually evaluated through metallography studies (Stobrawa et al., 2007; Cwjna and Roskosz, 2001; Frade-Drumond et al., 2014; Castillo and Marin, 1985; Dobrzański et al., 2007; González et al., 2015; Wojnar, 2016); grain size, distribution of contraction cavities and manufacturing processes, which affect the mechanical properties of the material, are commonly feasible determined from such techniques (De-Cooman and Speer, 2011; Dieter and Bacon, 1986).

Finally, a third aspect considered in the preparation of this report, is related to the choice of steel 1018, which is a sweet and low carbon steel widely known for its good combination of strength, ductility and hardness. Several contributions associated with mechanical properties and heat treatments have been reported for steel 1018 (Suzuki and Mcevely, 1979; Jayaraman et al., 1997; Topçu and Ubeyli, 2009; Doong and Tan, 1989; Clough et al., 2003; Akkurt et al., 1996). Being the most common steel of cold-rolled steel, it is a very useful product due to its typical characteristics of good mechanical strength and good ductility. In general terms, this metal has excellent weldability and better machinability than most carbon steels. Similarly, its alloy with tin (Noguez et al.,

2002) allows the strengthening of its mechanical properties, especially with respect to ductility.

The mechanical properties of 1018 steel, such as its hardness (126 HB), creep yield (370 MPa), maximum effort (440 MPa), modulus of elasticity (205 GPa) and machinability (76%), among other, make it ideal for a wide range of components such as pins, rods, shafts, gears and sprockets. While it is true that other steels can exceed their mechanical properties, the 1018 has the advantage of easier, machine-made production, presenting a low cost in the market.

The main objective of this report is to describe a methodology with educational research reference for the didactic evaluation of the main techniques for treatment of materials. Experimental work was realized with participation of student of investigative exercise, research assistantships and linkage projects as other learning modalities.

As part of the experience in academic training, it has been perceived that the study of heat treatments and properties of materials usually presents a certain level of difficulty in the students' learning, mainly due to the number of standards (ASTM, ASM), techniques and criteria in which is based. In this sense, the methodology provides a reference for the academic evaluation of the main techniques associated with the treatment of materials. The report includes experimental evaluations that allow identifying microstructure, mechanical properties, hardness and thermal treatments in samples machined according to the heat treater's guide (Harry, 1995).

MATERIALS AND METHODS

Sample preparation begins with cutting the specimen 1" in diameter and 1" in length. Subsequently, the sample is tilled with silicon carbide abrasive paper (sandpaper) number 80, 160, 240, 400, 600, 1000, and 2000, using water as lubricant and a flat surface as carrier. It should be noted that in each change of abrasive paper, the sample is rotated 90° so that the stripes generated are perpendicular to those generated by the new abrasive paper. After the AISI-SAE samples have been tilled, the polished process was applied, which consists of the elimination of all the stripes generated by the abrasive papers, using abrasive powder "alumina" of 3 microns and water as lubricant. Subsequently, the microstructure is cleaned and revealed by chemical attack with 5% Nital (5 ml nitric acid, 95 ml alcohol). Samples were cleaned with ethyl alcohol to remove residues and stains in the sample as indicated by ASTM standard (ASTM E3, 2017).

Different heat treatments were applied to AISI-SAE 1018 steel specimens (Chemical Composition: 0.15 to 0.20% C; 0.60 to 0.90 Mn; 0.04% P; 0.05% S) with a C401 H-PM3E Cress furnace. The temperature was raised at intervals of 250 to 930°C (Austenization temperature), according to Szykman et al. (2000) and Harry (1995).

*Corresponding author. E-mail: fmesa@uabc.edu.mx. Tel: (52) 664-756-3971.

Author(s) agree that this article remain permanently open access under the terms of the [Creative Commons Attribution License 4.0 International License](https://creativecommons.org/licenses/by/4.0/)

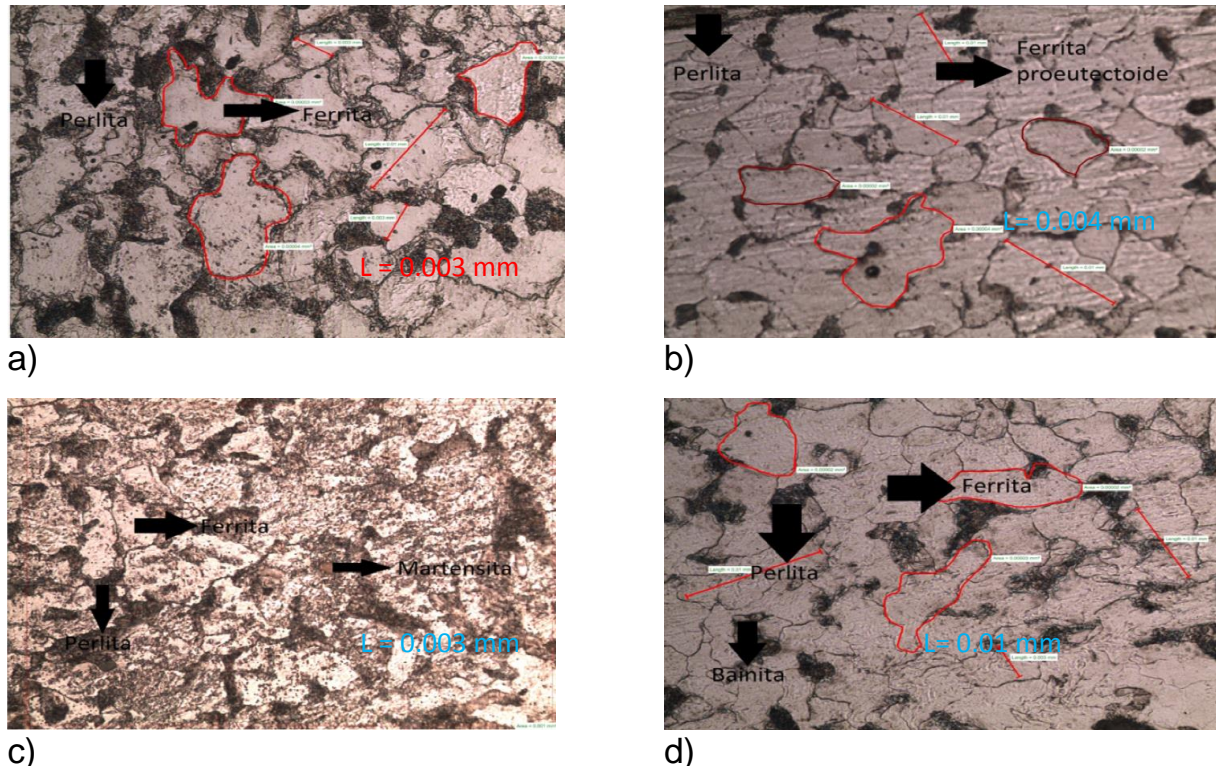


Figure 1. AISI-SAE 1018 steel attacked with 2% Nital in samples with metallographic processes (100x). The phases for control (a), annealing (b), normalized (c), and hardness (d) are shown. The lines marked in the images highlight the lengths and perimeter of the grains; the arrows identify the phases found in each of the samples.

Subsequently, the specimens were removed and the specific treatment was preceded. In the hardening treatment, they are immersed in water at room temperature for a sudden cooling; for the treatment of normalizing, the test tube is taken and left outdoors. The annealing process was realized placing the sample in the oven with a uniform cooling ramp until it reached the ambient temperature.

For the metallographic analysis, the polished samples were attacked with Nital 2% for 10 s in order to reveal the microstructure. Subsequently, the samples were cleaned with alcohol and observed in the metallographic microscope. The images were obtained with the help of the Nikon NIS Elements computer program (Laboratory Imaging, s.r.o., Za Drahou 171/17, cz-102 00 Praha 10, version 4.10.03). Images with different scales were obtained in order to observe the microstructure and identify the phases involved in each of the thermal treatments, according to ASTM E112 (ASTM E112, 2013) and ASM (Vander-Voort et al., 2004).

In order to perform the stress test on the different test specimens previously machined and according to the specifications of the American Society for Testing Materials ASTM (ASTM E8, 2016), these were subjected to annealing, normalizing and hardening heat treatments. The diameter and length of the calibrated area were dimensioned, as indicated by the standard protocols. Once the specimen was centered and held, *TrapeziumX* computer program (*Materials Testing Software TRAPEZIUM LITE X 349-02788E*) pre-loaded in the system, as well as the diameter and initial length for the development of the test were selected. The loading and displacement positions were tared and the test was performed in accordance with ASTM recommendations.

The metallographic treated samples were mounted and fixed in a

CV-600A "SPI" durometer for Rockwell A, B, C and F tests to figure perform the Rockwell B hardness test. For all sample analysis, 1/16 (1.59 mm) tungsten carbide round indenter was used. With 100 kg preload, as indicated by standards (ASTM E8, 2016; DIN-EN-ISO-6508, 2006; ASTM E18, 2017), the load was applied, obtaining the hardness reading on the cover of the durometer. Data were recorded and compared with the hardness range tables, according to literature (ASTM E1140, 2012). Once thermally treated samples were both prepared and conditioned, they were evaluated under ASTM E3 and ASTM E112 considerations.

RESULTS AND DISCUSSION

Figure 1 show the phases presented in AISI-SAE 1018 steel without heat treatment and with treatment at 100x. A metal matrix of ferrite (light zone) and pearlite (dark zone) for reference sample (cold rolled or control sample) can be observed (Figure 1a). The microstructure resulting from the heat treatment of annealing is observed in Figure 1b; that is, a metal matrix of ferrite and pearlite in the steel. Figure 1c describes the microstructure of annealing; this contains martensite and ferrite grains; while Figure 1d shows the effect of the normalized, where a metal matrix of ferrite can be seen, as well as in the limits of grain, pearlite. It should be noted that the formation of 100% martensite is only possible in very thin sections, as well as with a rapid cooling. On the other

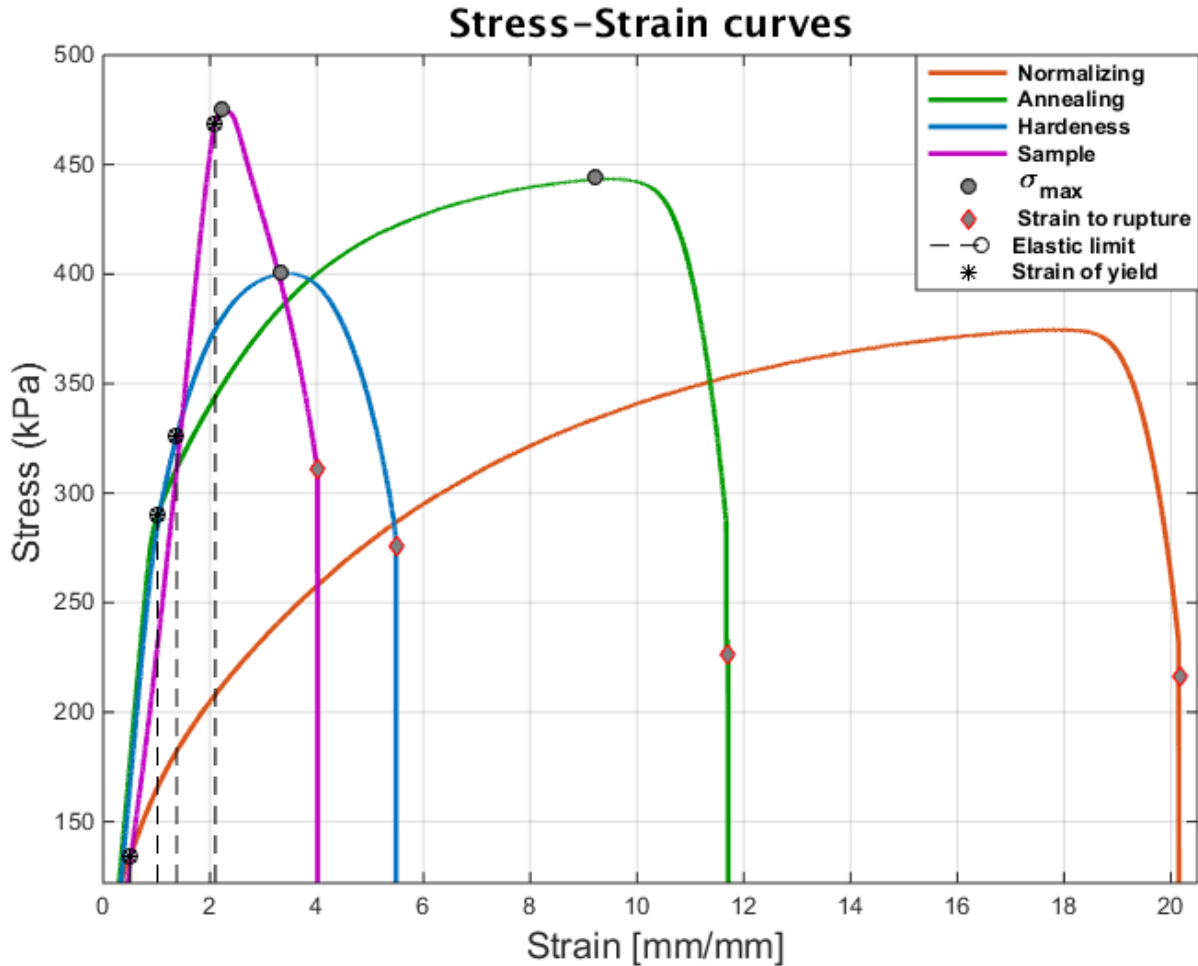


Figure 2. The stress-strain curves obtained from the tensile stress tests.

hand, diameter of the order of 3 to 4 μm can be observed in both the annealed samples (Figure 1b) and normalized (Figures 1d), associated to grain size ASTM 5 to 6 (ASTM E112, 2013), whereby the control sample is assumed to have a condition of normalized. The lines marked in the photographs of Figure 1 highlight the lengths and perimeter of the grains. The arrows identify the phases found in each of the samples.

With respect to the stress test, the comparison of the four stress-strain curves corresponding to each of the thermal treatments performed and the reference sample are recorded in the Figure 2, where it can be seen that the σ - ϵ curves corresponding to those tempered specimens show higher yield strength and lower elongation percentage. Similarly, the tenacity (area under the σ - ϵ curve) was higher in the normalized sample. The resilience (area under the curve σ - ϵ in the elastic zone delimited by the dotted line) was higher in the control sample. The annealed sample presented greater stress at rupture and the plastic zone was higher in the normalized sample; such plastic zone is delimited

between the dotted line and the break point in each of the curves.

The values of lengths, diameters, areas, stresses, Young's modulus, percentages of area reduction, elongation, as well as the resilience and average values of the hardness test obtained from measurements in the tensile and hardness tests were recorded in Table 1. Based on the results, it can be observed that in the normalized sample, the percentage of elongation was 67.75% and the area reduction was 79.3%, which indicate a greater tenacity. Also, the Young's modulus of 277.6 kPa turned out to be higher than the other thermally treated samples.

The annealing sample showed a higher maximum stress than the other samples with 444 kPa treatment. For the temperate sample, the maximum stress values were higher with respect to the rest of the samples, both in yield and in rupture, whose values correspond to 326.24 and 91.86 kPa, respectively. Likewise, the calculated resilience was the highest among the heat treated samples with a 223.52 kJ/m^2 .

Table 1. Results obtained from the stress-strain curve and the hardness tests.

Parameter	Normalizing	Annealing	Hardness	Sample
l_o (mm)	41.80	40.51	41.91	40.64
l_f (mm)	70.12	57.27	48.99	43.84
\varnothing_o (mm)	6.24	6.22	6.14	6.29
\varnothing_f (mm)	2.84	3.04	3.63	1.47
A_o (mm ²)	30.58	30.38	29.60	31.07
A_f (mm ²)	6.33	7.25	10.34	1.69
Rupture strength (kN)	1.37	2.93	4.22	5.54
E (kPa)	277.59	262.14	250.98	300.18
Strain of yield (kPa)	134.24	290.14	326.24	468.91
Strain at 0,2%	137.20	292.79	317.55	464.51
σ_{\max} (kPa)	374.71	444.09	400.65	475.50
Strain to rupture (kPa)	25.10	62.26	91.86	114.75
% of elongation	67.75	41.37	16.9	7.87
% of area reduction	79.3	76.13	65.06	94.56
Resilience (kJ/m ²)	33.92	151.53	223.52	504.37
Average HRB (100 kg, 1/16)	11.8	17.8	73.8	14.6

A_o , Initial cross-sectional area; A_f , Final area of the cross-section area at the surface of the fracture; σ , Effort; ϵ , Unitary deformation; E, Young's Module; δ , Elongation; \varnothing , Diameter; P, Force/Load; l_o , Initial length of the calibrated zone; l_f , Final length of the calibrated zone; $\dot{\epsilon}$, Strain speed; ANSI, American National Standards Institute; SAE, Society of Automotive Engineers; ASTM, American Society for Testing Materials; ASM, American Society for Metals; HRB, Hardness Rockwell B; ISO, International Organization for Standardization.

The tempering heat treatment at 930°C for 1 h and with sudden cooling, allows the steel to present more defined characteristics as the greater Modulus of Elasticity, greater ultimate strength, and a greater yielding stress due to the martensite phase (Figure 1d), corresponding to the tempering, values that are congruent with the hardness values. This normalized thermal treatment, but with cooled in the open air, allowed an increase in the ductility and, consequently, its deformation was greater and the yielding effort was low; that is to say, it had less elastic deformation and increased plastic deformation. Given the characteristics obtained in each of the thermal treatments made of steel, it can be concluded that the reference sample has a normalized condition. Based on the circumstances foreseen in the study, the mechanical properties of the AISI-SAE 1018 steel can be correlated with the values of tension; hardness and microstructure differ with respect to the applied heat treatment.

Conclusion

The periodic curricula updating at different levels of education is an evidence of the national effort to improve the skills of engineering graduates. Although the development of traditional courses at different engineering areas continues to be one of the main tools to ensure the preparation of engineers, the implementation of other teaching modalities such as investigative exercise, research assistantships and linkage projects implemented through methodology under

study, promote a more direct approach of the student with the technology, motivating their level of participation and professional strengthening.

The mechanic engineering field is centered on a significant number of international norms and regulations associated with testing and evaluations of materials properties, so that students are called to review a number of manuals that allow them to take advantage of equipment and resources. Therefore, the student of engineering requires the consultation of sources that aid mediates between articles of very specialized essays, theoretical courses and manuals of considerable extent, as well as extracurricular activities that allow him/her to develop other competencies associated with the management of techniques and its interpretations.

The study was centered in an educational research emphasis about the material microstructure as well as of the heat treatments in samples machined according to ASTM E8 specifications. The experimental process was developed within the laboratory practice programs for physical and mechanical engineering students of a prestigious university at the pacific.

The methodology provides a reference for the academic evaluation of the main techniques associated with the treatment of materials. The results obtained and the experimental schemes developed describe the correlation between the microstructure and the mechanical properties as a fundamental tool for the comprehension of the treatment of materials in diverse areas of engineering. For the steel AISI-SAE 1018, it was determined that the heat treatment makes possible the

change in the mechanical properties of the material, which can be observed in the tests of tension and hardness, as well as metallographic analysis.

The report is an academic reference respect to the experimental mechanical engineering training in an institution of higher education studies at USA-Mexico border.

CONFLICT OF INTERESTS

The authors have not declared any conflict of interests.

ACKNOWLEDGMENTS

The authors express their thanks to the Secretariat of Public Education through the Professor' Improvement Program (PRODEP), for the financial support. Research was conducted throughout the Mechanical Systems Optimization Academic Group (UABC-CA-219). The authors are grateful for the excellent collaboration of Dr. Arturo Baundez Pliego, CENIDET: National Center for Research and Technological Development.

REFERENCES

- Akkurt AS, Akgün OV, Yakupoglu N (1996). The effect of post-heat treatment of laser surface melted AISI 1018 steel. *J. Mater. Sci.* 31(18):4907-4911.
- ASTM E112-13 (2013). Standard test methods for determining average grain size. ASTM International. West Conshohocken. PA. <https://doi.org/10.1520/E0112>
- ASTM E1140-12b (2012). Standard Hardness Conversion Tables for Metals Relationship Among Brinell Hardness Vickers Hardness, Rockwell Hardness, Superficial Hardness, Knoop Hardness, Scleroscope Hardness, and Leeb Hardness. ASTM International. West Conshohocken. PA. <https://doi.org/10.1520/E0140>
- ASTM E18-17e1 (2017). Standard Test Methods for Rockwell Hardness and Rockwell Superficial Hardness of Metallic Materials. ASTM International, West Conshohocken. PA. <https://doi.org/10.1520/E0018-17E01>
- ASTM E3-11 (2017). Standard Guide for Preparation of Metallographic Specimens. ASTM International, West Conshohocken. PA. <https://doi.org/10.1520/E0003-11R17>
- ASTM E8/E8M-16a (2016). Standard test methods for tension testing of metallic materials. ASTM International. West Conshohocken. PA. https://doi.org/10.1520/E0008_E0008M-16A
- ASM International Handbook Committee (2014). ASM Handbook: Heat treating -Volume 4D: Heat Treating of Irons and Steels. ASM International.
- Atman CJ, Adams RS, Cardella ME, Turns J, Mosborg S, Saleem J (2007). Engineering design processes: A comparison of students and expert practitioners. *J. Eng. Educ.* 96(4):359-379.
- Calik A (2009). Effect of cooling rate on Hardness and Micro structure of AISI 1020, AISI 1040 and AISI 1060 steels. *Int. J. Phys. Sci.* 4(9):514-518.
- Castillo FJ, Marin J (1985). Metallographic study of formed metallic uranium. *Nucleotecnica* 4(8):19-27.
- Clough RB, Webb SC, Armstrong RW (2003). Dynamic hardness measurements using a dropped ball: with application to 1018 steel. *Mater. Sci. Eng. A.* 360(1):396-407.
- Cwjna J, Roskosz S (2001). Effect of microstructure on properties of sintered carbides. *Mater. Charact.* 46(2-3):197-201.
- Daramola OO, Adewuyi BO, Oladele IO (2010). Effects of heat treatment on the mechanical properties of rolled medium carbon steel. *J. Miner. Mater. Charact. Eng.* 9(08):693-708.
- Daunton C, Kothari S, Smith L, Steele D (2012). A history of materials and practices for wound management. *Wound Pract. Res. J. Austr. Wound Manag. Assoc.* 20(4):174-176.
- De-Cooman BC, Speer JG (2011). Fundamentals of steel product physical metallurgy. AIST. Warrendale. PA.
- Dieter GE, Bacon DJ (1986). Mechanical metallurgy –Vol:03. New York: McGraw-Hill.
- DIN-EN-ISO-6508 (2006). Metallic Materials–Rockwell Hardness Test. ISO. Berlin-Germany.
- Dobrzański LA, Tański T, Čížek L (2007). Heat treatment impact on the structure of die-cast magnesium alloys. *J. Achiev. Mater. Manuf. Eng.* 20(1-2):431-434.
- Doong JL, Tan YH (1989). Effect of laser surface alloying chromium onto AISI 1018 steel on the fatigue crack growth rate. *Int. J. Fatigue* 11(4):239-247.
- Dym CL, Agogino AM, Eris O, Frey DD, Leifer LJ (2005). Engineering Design Thinking, Teaching, and Learning. *Int. J. Eng. Educ.* 94(1):103-120.
- Dutson AJ, Todd RH, Magleby SP, Sorensen CD (1997). A Review of Literature on Teaching Engineering Design Through Project-Oriented Capstone Courses. *Int. J. Eng. Educ.* 86(1):17-28.
- Fadare DA, Fadara TG, Akanbi OY (2011). Effect of heat treatment on mechanical properties and microstructure of NST 37-2 steel. *J. Miner. Mater. Charact. Eng.* 10(03):299-308.
- Frade-Drumond AL, Abdalla AJ, de Moura-Neto C, Manabu-Hashimoto T, de Oliveira-Hein LR (2014). Mechanical characterization of a steel AISI 43100 submitted to different routes of heat treatments. *Mater. Sci. Forum. Trans. Tech. Publications* 802(1):373-376.
- González AG, Muñoz CA, Arnaldo GJ (2015). Metallographic Study on Alloy Zircaloy-4 of Nuclear Use. *Procedia Materials Sci.* 8(1):494-501.
- Harry C (1995). Heat Treating Guide: Practice and Procedures for Irons and Steels. ASM International. 2Ed.
- He P, Jia D, Lin T, Wang M, Zhou Y (2010). Effects of high-temperature heat treatment on the mechanical properties of unidirectional carbon fiber reinforced geopolymer composites. *Ceram. Int.* 36(4):1447-1453.
- Ikpeseni SC, Onyekpe BO, Momoh IM (2015). Effect of tempering on the microstructure and mechanical properties of austenitic dual phase steel. *Int. J. Phys. Sci.* 10(16):490-497.
- Jayaraman A, Cheng ET, Earthman JC, Wood TK (1997). Axenic aerobic biofilms inhibit corrosion of SAE 1018 steel through oxygen depletion. *Appl. Microbiol. Biotechnol.* 48(1):11-17.
- Kuśrowski P, Sułkowska D, Chmielarz L, Rafalska-Łasocha A, Dudek B, Dziembaj R (2005). Influence of thermal treatment conditions on the activity of hydrotalcite-derived Mg–Al oxides in the aldol condensation of acetone. *Microporous Mesoporous Mater.* 78(1):11-22.
- Mills JE, Treagust DF (2003). Engineering education-Is problem-based or project-based learning the answer. *Australas. J. Eng. Educ.* 3(2):2-16.
- Noguez ME, Balderas JE, Robert T, Ramirez J, Salas G (2002). Propiedades mecánicas de aceros de bajo carbono con estaño y diferentes contenidos de elementos residuales. *Rev. Cienc. Ing.* 23(3):31-35.
- Parkinson A (1995). Robust mechanical design using engineering models. *J. Vib. Acoust.* 117(B):48-54.
- Schaefer D, Panchal JH, Choi SK, Mistee F (2008). Strategic Design of Engineering Education for the flat world. *Int. J. Eng. Ed.* 24(2):274-282.
- Selfridge AR (1985). Approximate material properties in isotropic materials. *IEEE Trans. Sonics Ultrason.* 32(3):381-394.
- Stobrawa JP, Rdzawski ZM, Gluchowski W (2007). Structure and properties of dispersion hardened submicron grained copper. *J. Achiev. Mater. Manuf. Eng.* 20(1):195-198.
- Suzuki A, Mcevely AJ (1979). Microstructural effects on fatigue crack growth in a low carbon steel. *Metall. Mater. Trans. A.* 10(4):475-481.
- Szykman S, Sriram RD, Bochenek C, Racz JW, Senfaute J (2000). Design Repositories: Engineering Design's New Knowledge Base. *IEEE Intell. Syst. Appl.* 15(3):48-55.

- Topçu O, Übeyli M (2009). On the microstructural and mechanical characterizations of a low carbon and micro-alloyed steel. *Mater. Des.* 30(8):3274-3278.
- Vander-Voort GF, Lampman SR, Sander BR, Anton GJ, Polakowski C, Kinson J, Scott-Jr WW (2004). *ASM handbook. Metallography and Microstructures* 9:44073-0002.
- Whitesides GM, Wong AP (2006). The intersection of biology and materials science. *MRS Bull.* 31(1):19-27.
- Williams JC, Starke EA (2003). Progress in structural materials for aerospace systems. *Acta Mater.* 51(19):5775-5799.
- Wojnar L (2016). Application of ASTM standards in quantitative microstructure evaluation. *Czasopismo Techniczne. Mechanika Zeszyt 4-M 2016.* pp. 41-46.

Full Length Research Paper

Intersection of lineaments for groundwater prospect analysis using satellite remotely sensed and aeromagnetic dataset around Ibodi, Southwestern Nigeria

Ilugbo S. O.* and Adebisi A. D.

Department of Applied Geophysics, Federal University of Technology, Akure, Ondo State, Nigeria.

Received 13 October, 2017; Accepted 28 November, 2017

This research investigates groundwater potential of Ibodi and its environs using satellite imagery remotely sensed and aeromagnetic dataset. This hydrogeological investigation involved the extraction of lineaments from Landsat Thematic Mapper (TM) satellite imagery and aeromagnetic lineament of the area. The processed image revealed lineaments trending in approximately NE-SW direction; also, Landsat and aeromagnetic lineament trends tend to agree in the study area, suggesting real continuous fractures at depth. Hydrogeological maps, based on lineament and lineament intersection were produced from the generalized lineament trends in the area. The lineament intersection density map identified cluster zones in the range of 0 to 1.17, 1.17 to 2.34, 2.34 to 3.52, 3.52 to 4.69 and 4.69 to 5.86 kg/kg², respectively. The map showed that the concentrations of lineament intersection nodes dominate the eastern and north-eastern parts of the study area while other areas are characterized by scanty or no lineament intersections nodes. The lineament analysis has been effectively done in a geographic information system (GIS) environment. Results from the vertical electrical sounding (VES) data reveals that the areas where the lineament intersected has tendency of very high groundwater prospect which reflects that the area will be good for groundwater development. The study thus displays that the remote sensing and aeromagnetic technique is capable of extracting lineament trends in an inaccessible tropical forest and has led to the delineation of areas where groundwater occurrences are most promising for sustainable supply.

Key words: Geology, landsat lineaments, aeromagnetic lineaments, lineament intersections, geographic information system (GIS).

INTRODUCTION

Groundwater is one of the most valuable natural resources on the earth surface and serves as main

sources of drinking water. Basement complex have problem of potable groundwater supply due to the

*Corresponding author. E-mail: bussytex4peace44@gmail.com.

crystalline nature of the underlying rock which lack primary porosity (Olorunfemi and Fasuyi, 1993).

Groundwater storage capacity in those areas depends on the depth of weathering and the intensity of fracturing of the underlying rock. For basement rocks to become good aquifers, they must be highly fractured and highly weathered. Thickness of the weathered overburden and fractured zone determined the nature and intensity of hydrodynamic activities within the usually discrete bodies of aquifer in the terrain (Amudu et al., 2008; Amadi and Olasehinde, 2010).

Groundwater in crystalline rocks that have no intergranular porosity moves in a connected fracture network; but far from all fractures are permeable, and fracture permeability varies considerably (Banks et al., 1996). It is generally recognized that, in the prospect area of faults and fracture lineaments, the fault core and central zone have low permeability while the outer damage zone has enhanced permeability compared with the surroundings (Caine et al., 1996; Evans et al., 1997; Henriksen and Braathen, 2006). Lineament mapping was used long before this work in other geological applications and the first usage of the term lineament in geology is probably from a paper by Hobbs (1904, 1912), who defined lineaments as significant lines of landscape caused by joints and faults, revealing the architecture of the rock basement. This was later used by O'Leary et al. (1976) as a basis for developed definitions. Lineament is a mappable linear or curvilinear feature of a surface whose parts align in a straight or slightly curving relationship (Hung et al., 2005). They may be an expression of a fault, joints or other line weakness. These features are mappable at various scales, from local to regional, and can be utilized in mineral, hydrocarbons, and groundwater explorations. This interest has grown most rapidly in geological studies since the introduction of aerial photographs and satellite images. Generally, lineaments are underlain by zones of localized weathering and increased permeability and porosity. Meanwhile, some researchers studied relationships between groundwater productivity and the number of lineaments within specifically designated areas or lineament density rather than the lineament itself (Hardcastle, 1995).

This research focuses on intersecting landsat lineament and aeromagnetic lineament for regional groundwater prospect evaluation. Lineament intersections represent nodal point for two or more lineament lines (Bayowa et al., 2014). The nodes of intersections are the point of interest which indicate site for appreciable groundwater accumulation.

Study location and geology

Ibodi and its environs comprises sixty-eight villages which are located on the crystalline basement complex

and falls within latitude 7° 32' 20" to 7° 38' 20" North and longitude 4° 36' 20" to 4° 44' 20" East (Figure 1). This area falls within the 1:50,000 topographic map of Ilesa sheet 234 SW. Major and minor road linkages characterize the study area linking both towns and villages together. In general, the location can be said to be fairly accessible with footpaths in areas where there are neither major nor minor roads. Regionally, the study area belong to the Southwestern Nigeria basement complex comprising migmatite-gneiss complex, metaigneous rock such as pelitic schist, quartzite, amphibolites, charnockitic rocks, older granite and unmetamorphosed dolerite dykes. The rock sequence consists of basically weathered quartzite of older granite. The basement complex rocks of Nigeria are made up of heterogeneous assemblages (Rahaman, 1976). The geology of Ibodi and its environs is mainly Precambrian Basement rock (Figure 2) because of the tectonics and metamorphic changes that has occurred in the area (Olade, 1978). Schist and amphibolites, magnetite - gneiss undifferentiated and amphibolites stands out in the Basement rock of the investigated area.

METHODOLOGY

The work utilized remote sensing, aeromagnetic and electrical resistivity data in the assessment of groundwater prospect around Ibodi, Osun State.

The remote sensing data (Landsat imagery) were acquired from the Global Land Cover Facility homepage and the automatic lineament extraction process was carried out using "ENVI" 4.5, "Geomatical" pcl and "ArcGIS" 10.2 software which was used for digital image processing and lineament extraction from the satellite imageries. The aeromagnetic data was acquired from Nigerian Geological Survey Agency and the data set gridded using minimum curvature gridding method with 50 m cell size to produce total magnetic intensity map. Data enhancement techniques involving Butterworth filter, reduction to equator and derivative filters were applied to the magnetic intensity map using Oasis Montaj 6.4.2 software package (Montaj TM Tutorial, 2004). 3D Euler deconvolution data assisted in determining the locations and depths of the geologic sources. Structural index of 1.0 was found appropriate for delineation of structures that are favourable for groundwater accumulation. Lineaments were generated by georeferencing and digitizing 3D Euler deconvolution results. A total of nine Vertical Electrical Sounding involving Schlumberger arrays were used to acquire depth sounding data in the investigated area with the apparent resistivity values obtained from the area plotted on bi-log graph against the current electrode separation spacing. The initial quantitative interpretations were made using partial curve matching technique in which the field curves produced or generated were matched segment by segment with the appropriate master curves and auxiliary curves. The resistivities and thicknesses of the various layers were improved upon by employing an automatic iterative computer program following the main ideas of Zohdy and Martin (1993). The WINRESIST computer software was employed for carrying out the iteration and inversion processes. Intersection of landsat lineament and aeromagnetic lineament density were used to determine the groundwater prospect of the area. A total of nine (9) vertical electrical sounding obtained within the study area were used to validate lineament intersections in order to ascertain the significances in term of groundwater prospect.

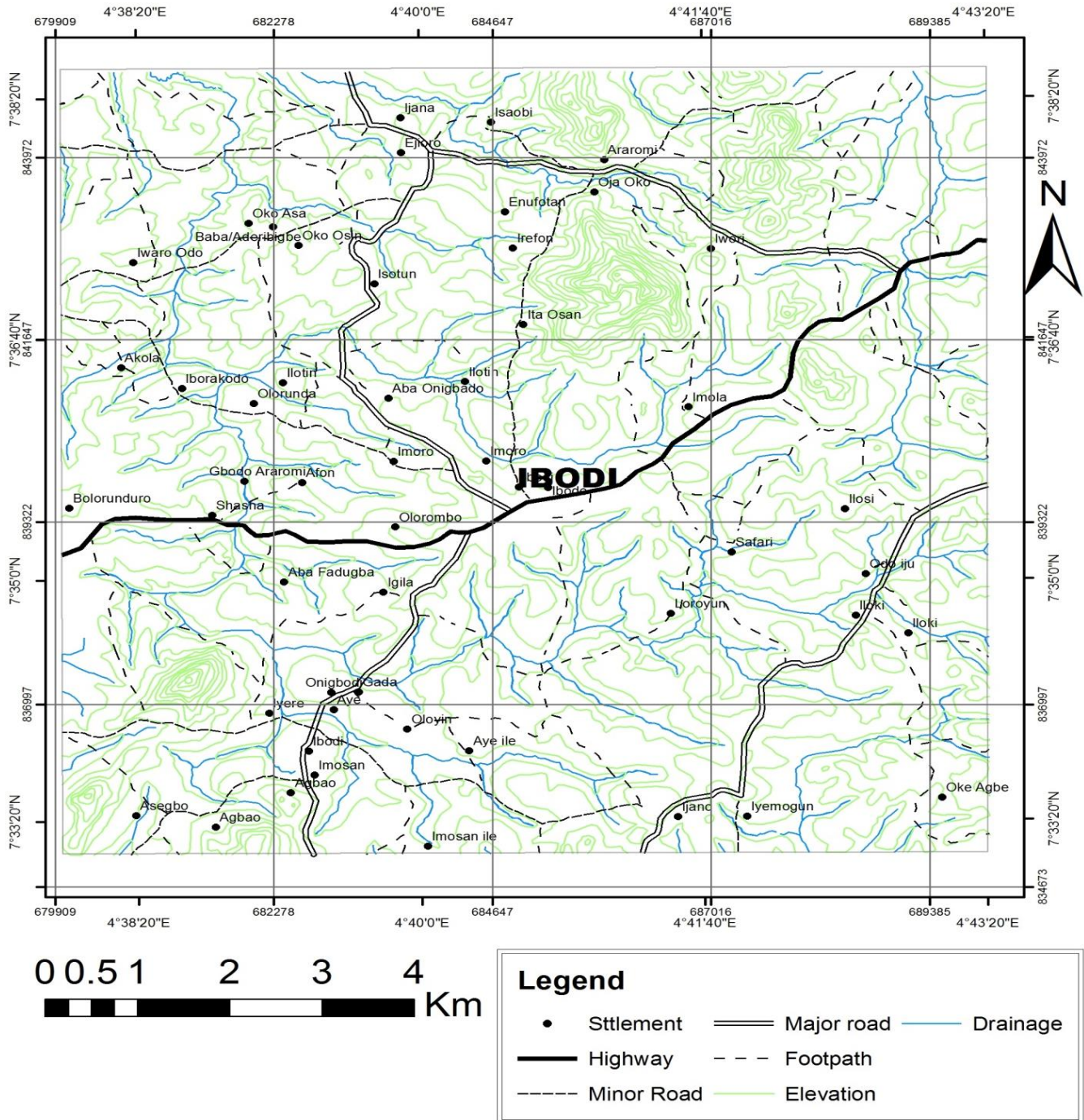


Figure 1. Location map of Ibodi and its environ showing the study area (after Osun State Ministry of Lands and Physical Planning 1965.Topographic Map of Ilesha SW sheet 234).

RESULTS AND DISCUSSION

Remote sensing

Lineament analysis from landsat imagery

Results obtained from the satellite image interpretation

(Figure 3) are discussed to demonstrate the usefulness of remote sensing in lineament mapping and analysis, that is, to delineate zones that are prone to groundwater development in the study area. The map shows that the northeastern region is characterized by very high concentration of lineaments, whereas the central parts of the study area are characterized by moderately

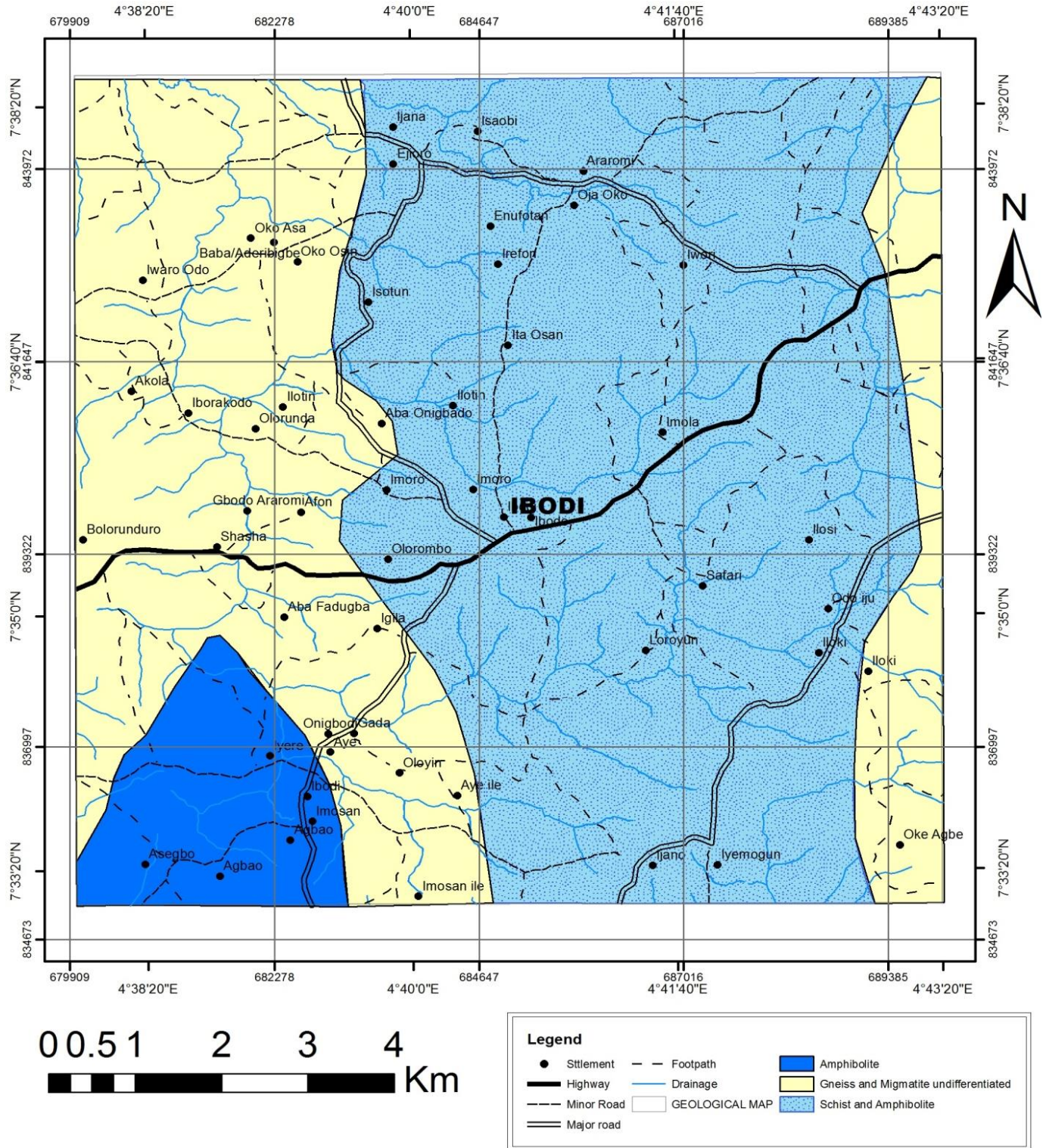


Figure 2. Geological map of Ibodi and its environs (after Osun State Ministry of Lands and Physical Planning 1980. Geological Survey of Ilesha Iwo Shist 60).

concentration of lineaments while the northwestern and the southeastern parts have low to very low concentration

of lineaments. The rose (azimuth-frequency) diagram of the lineaments (Figure 4) was prepared from the

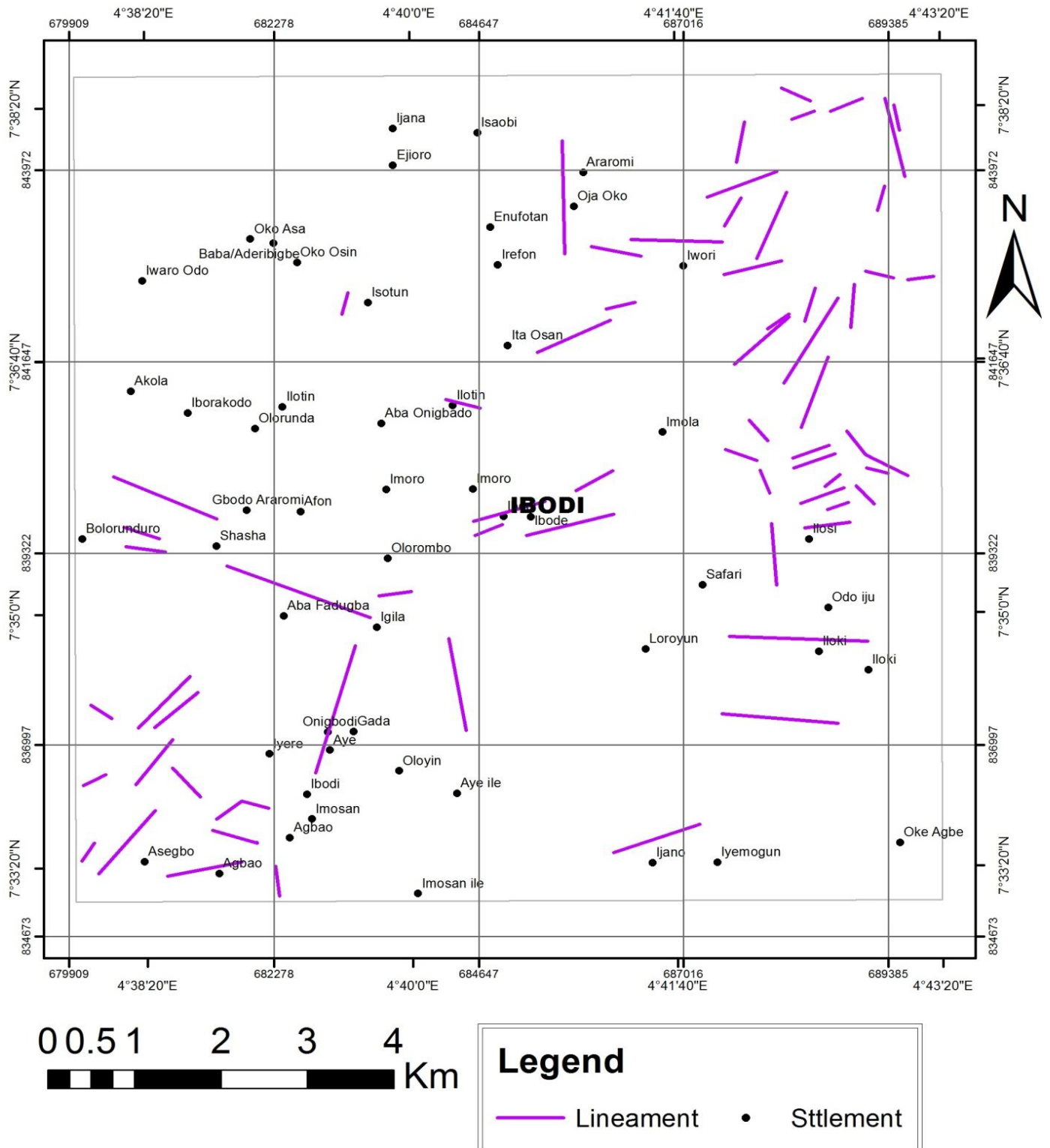


Figure 3. Landsat lineaments map of the study area.

extracted lineaments on the imagery which showed that there are three predominant sets of lineament which are closely related to tectonic activities such as

fractures, faults and joints in the study area. The lineaments trends in the NE-SW, ENE-WSW and NW-SE directions.

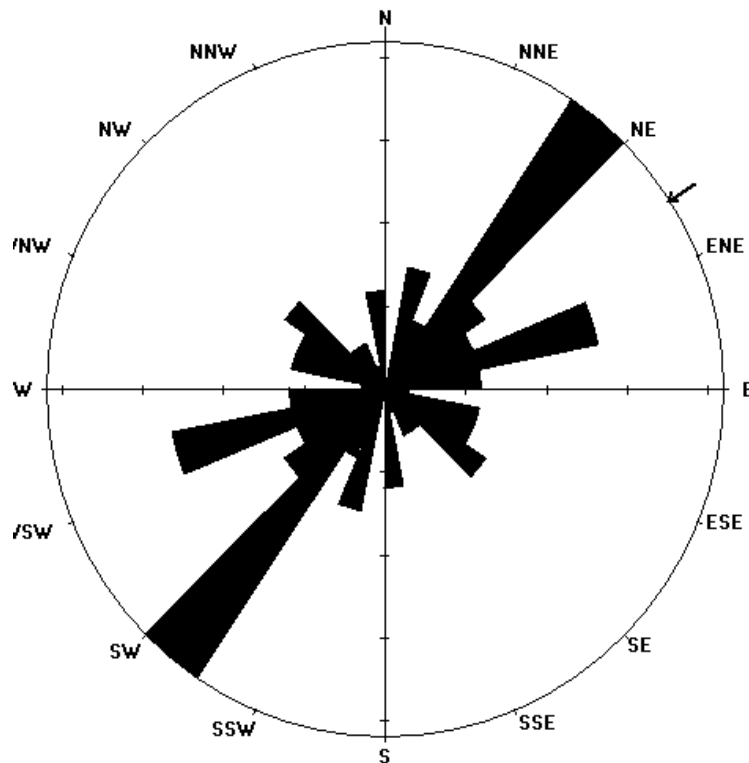


Figure 4. Rose (Azimuth-frequency) diagram of landsat lineaments orientations.

Landsat lineament on topographical and geological map

Figures 5 and 6 show landsat lineament on topographical and geological maps. Figure 5 shows that the northeastern parts, majority of the lineaments fall within the high hill with elevation between 380 m to 420 m and also at the southwestern part. Areas with high lineament density excluding (the residual hill environment) are good for groundwater development. Figure 6 show that there are more concentrations of lineaments on schist and amphibolites at the northeastern parts followed by amphibolites at the southwestern part while there exist scanty or low concentration of lineaments on gneiss and migmatite undifferentiated. This implies that there are more fracturing on schist and amphibolites, followed by amphibolites and gneiss and migmatite undifferentiated. Regarding groundwater exploration, these aforementioned areas may have high groundwater potentials due to their high concentration of lineaments, that is, since groundwater occurs within faults and fractures in the basement rock.

Landsat lineament density map

The lineament density of Ibodi and its environ was

computed based on the number of lineaments per unit area (kg/kg^2) of grid, for quick graphical assessment of the lineament density values of the area. Areas with high lineament density excluding (the residual hill environment) are good for groundwater development. Figure 7 shows five different hydrogeological potential zones distributed as patches in the study area. The zones are summarized in Table 1. The lineament density map shows that the lineament density is high around areas like Ibodi, Iloki, Iwori, Ijano, Ilotin, Aye, Igila, Agbao, Araromi and Oja Oko when compared to other areas in the study area.

Aeromagnetic data

Lineament analysis using 3D Euler deconvolution

3D Euler solution using structural index ($S.I = 1$) was applied to the aeromagnetic data for lineament analysis (Figure 8). The delineated solutions were extracted and digitized to produce the lineaments from magnetic data (Figure 9). The rose (azimuth-frequency) diagram of the lineaments (Figure 10) was prepared from the extracted lineaments on the aeromagnetic structures which shows that there are two predominant sets of lineament which are closely related to tectonic activities such as fractures,

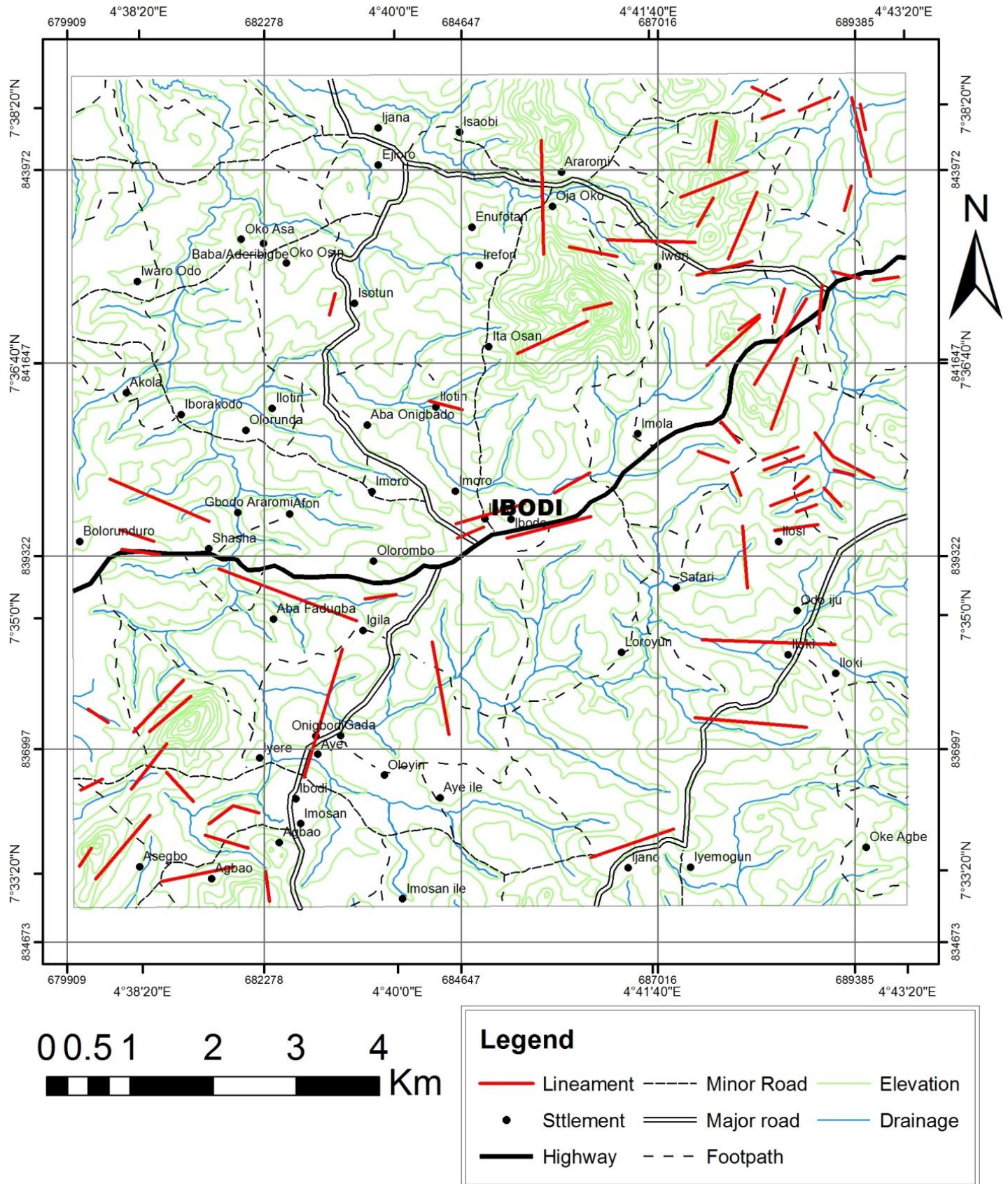


Figure 5. Landsat lineaments on topographical map of the study area.

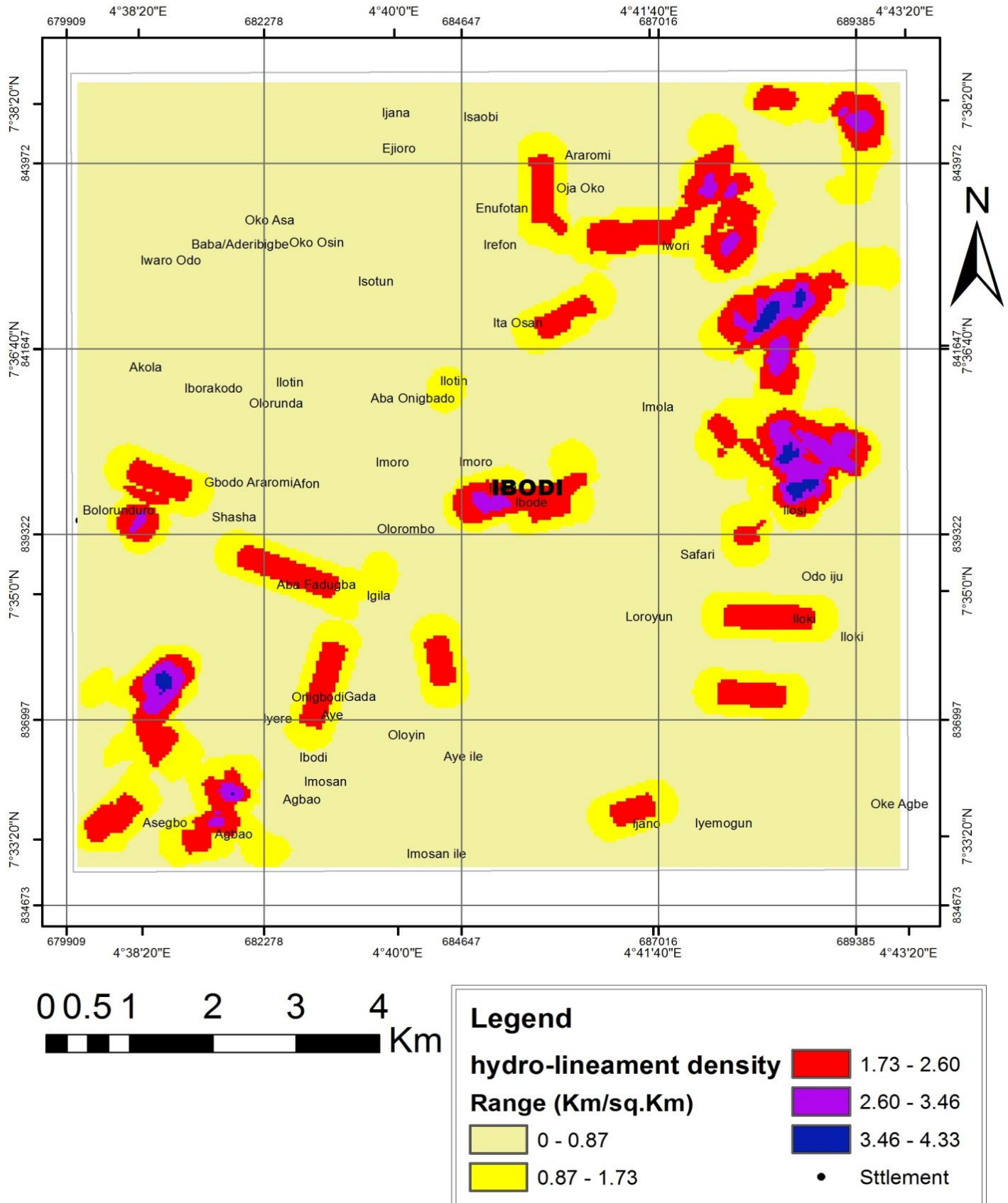
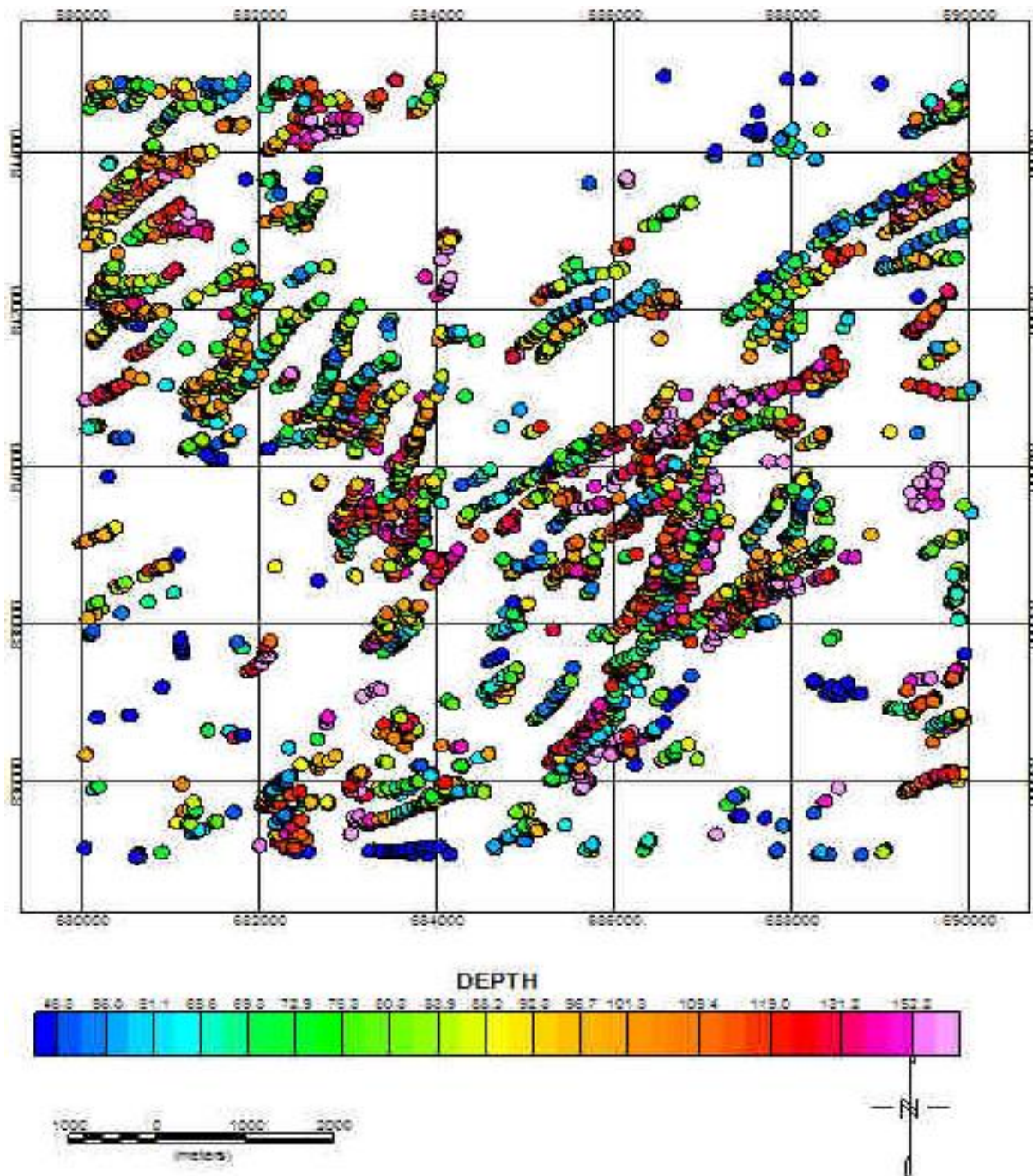


Figure 7. Landsat lineament density map of the study area.

Table 1. Groundwater prospecting of the study area based on landsat lineament density.

Lineament Density Colour Code	Lineaments Density Range (kg/kg^2)	Groundwater Prospecting
Lemon	0 – 0.87	Very low
Yellow	0.87 – 1.73	Low
Red	1.73 – 2.60	Moderate
Pink	2.60 – 3.46	High
Blue	3.46 – 4.33	Very high

**Figure 8.** 3D Euler solution from the analysis the aeromagnetic data over the study area with structural index (S.I = 1).

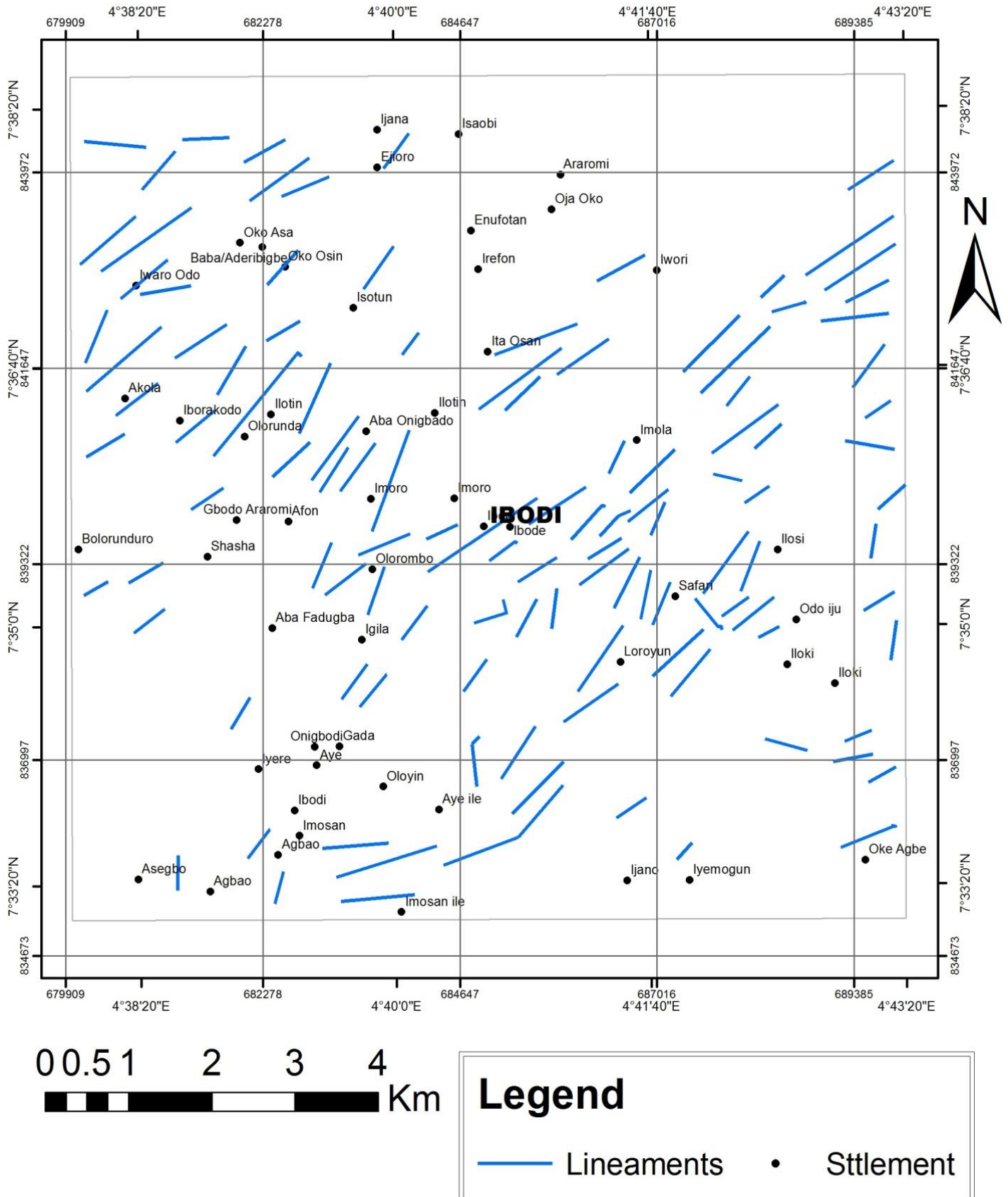


Figure 9. Aeromagnetic lineaments of the study area.

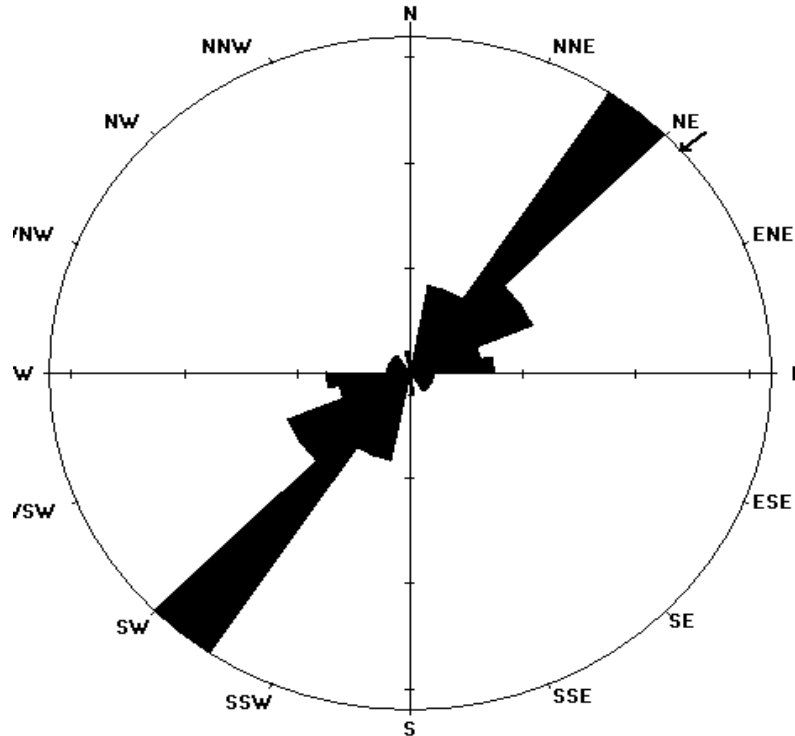


Figure 10. Rose (Azimuth-frequency) diagram of aeromagnetic lineaments orientations.

faults and joints in the study area. The lineaments trends NE-SW and ENE-WSW directions. Here it indicates more fracturing towards the NE direction suggesting comparatively more potential groundwater zone and hence better prospect for groundwater availability.

Aeromagnetic lineaments on topographical and geological map

Figures 11 and 12 displays aeromagnetic lineament on topographical and geological map. Figure 11 reveals that the majority of the lineaments fall within the plain land unlike surface lineaments (Landsat Lineament) which fall within the high hill. This implies that we cannot base our presumption on surface lineament without ascertaining it with subsurface lineaments in order to have clearer pictures of the groundwater prospect within the study area. Figure 12 shows that there are more concentration of lineaments on schist and amphibolites at the southeastern parts which go along with the landsat lineaments on geological map followed by gneiss and migmatite undifferentiated at the northwestern parts, while showing scanty or low concentration of lineaments on amphibolite. This implies that, there are more fracturing on schist and amphibolites. Regarding groundwater exploration, these aforementioned areas may have high groundwater potentials due to their high

concentration of lineaments, that is, since groundwater occurs within faults and fractures in the basement rocks.

Aeromagnetic lineament density map

Lineament density map is one of the important maps prepared from the lineaments, which are critically used in groundwater studies related to hard rock terrain, Figure 13 displays the aeromagnetic lineament density map of the study area. The map reveals five different hydrogeological potential zones distributed as patches in the study area. The zones are summarized in Table 2. The lineament density map reflects that the lineament density is high around areas like Ibodi, Iworo Odo and Sefari, when compared to other areas in the study area. Regarding groundwater exploration, these aforementioned areas may have high groundwater potentials due to their high concentration of lineaments, that is, since groundwater occurs within faults and fractures in the basement rocks.

Intersection of lineaments

Intersection of aeromagnetic and landsat lineaments

Figure 14 indicates the lineament intersection map

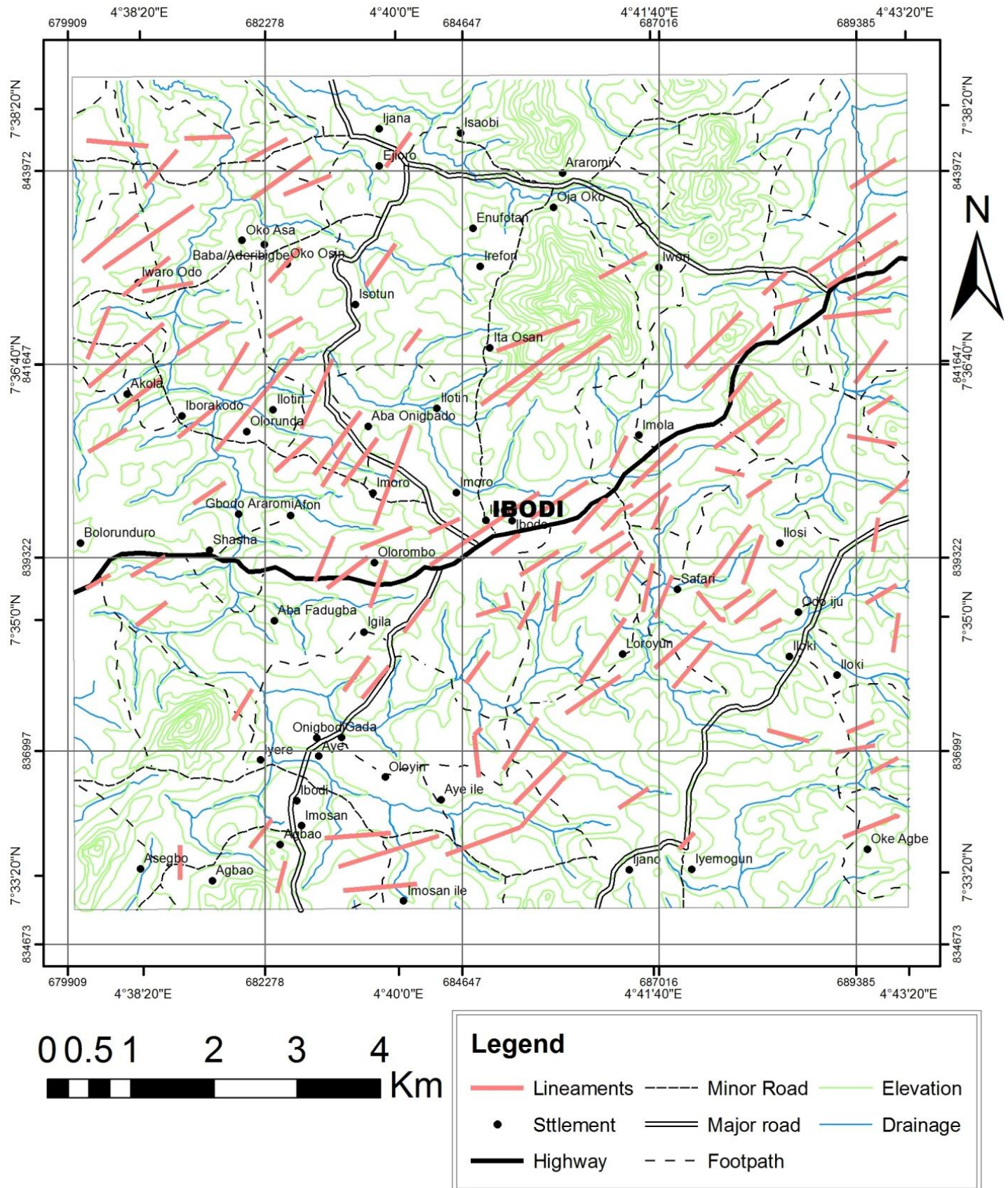


Figure 11. Aeromagnetic lineament on topographical map of the study area.

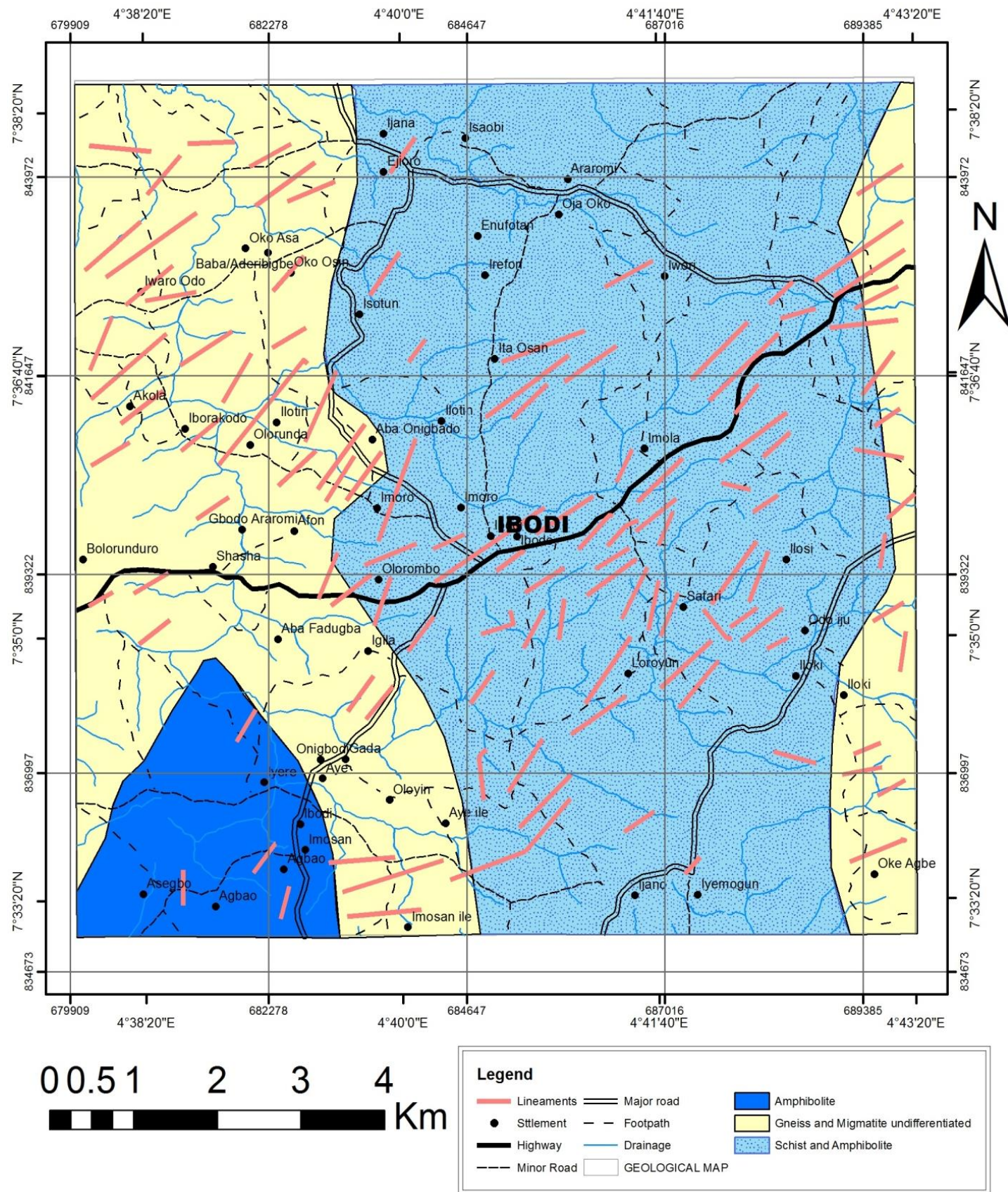


Figure 12. Aeromagnetic lineament on geological map of the study area.

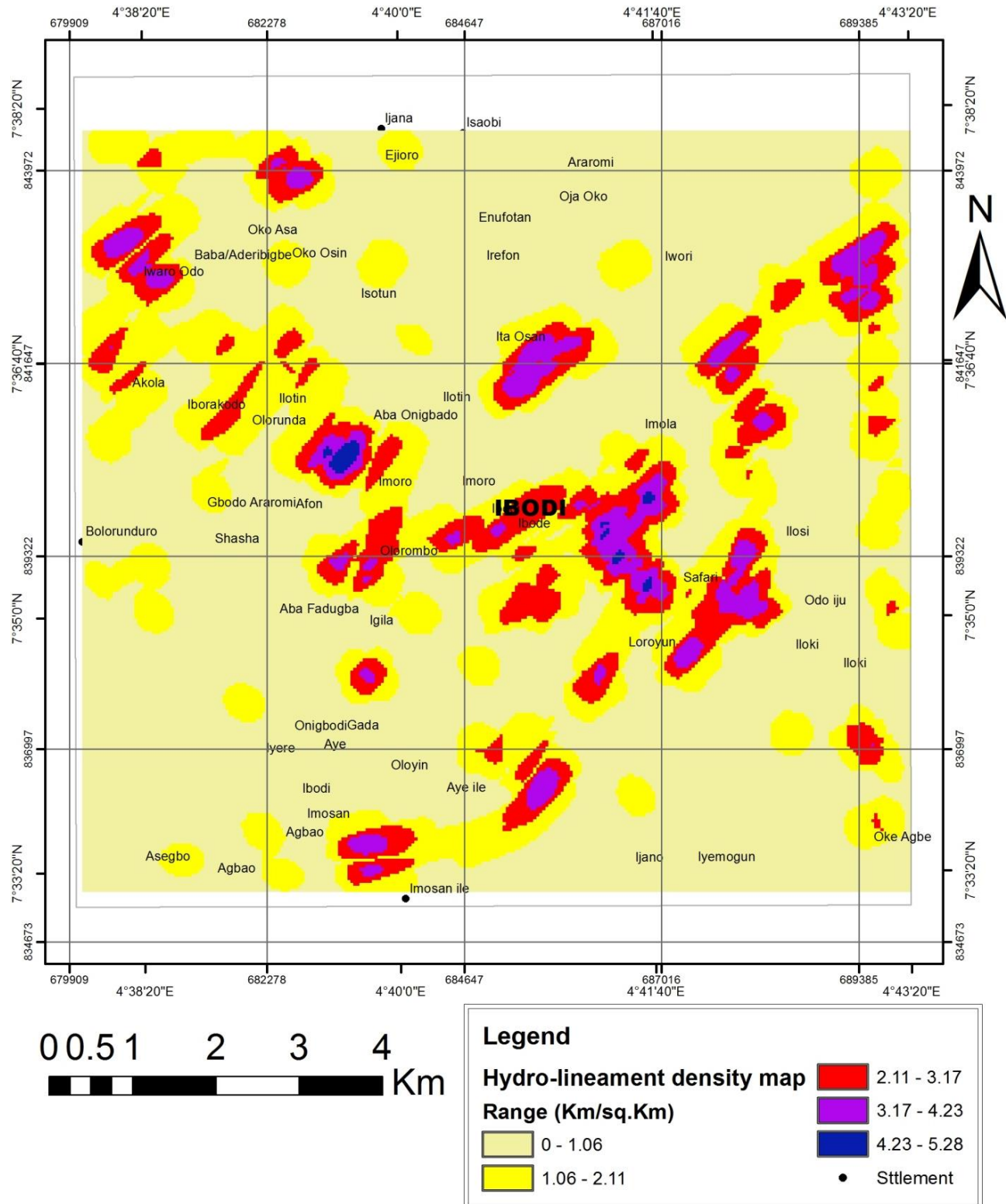


Figure 13. Aeromagnetic lineament density map of the study area.

between aeromagnetic lineaments and landsat lineaments of the study area. Lineament intersections are

potential site for appreciable groundwater accumulation. Lineament intersections represent nodal point for two or

Table 2. Groundwater prospecting of the study area based on aeromagnetic lineament density.

Lineaments Density Colour Code	Lineaments Density Range (kg/kg ²)	Groundwater Prospecting
Lemon	0 – 1.06	Very Low
Yellow	1.06 – 2.11	Low
Red	2.11 – 3.17	Moderate
Pink	3.17 – 4.23	High
Blue	4.23 – 5.28	Very High

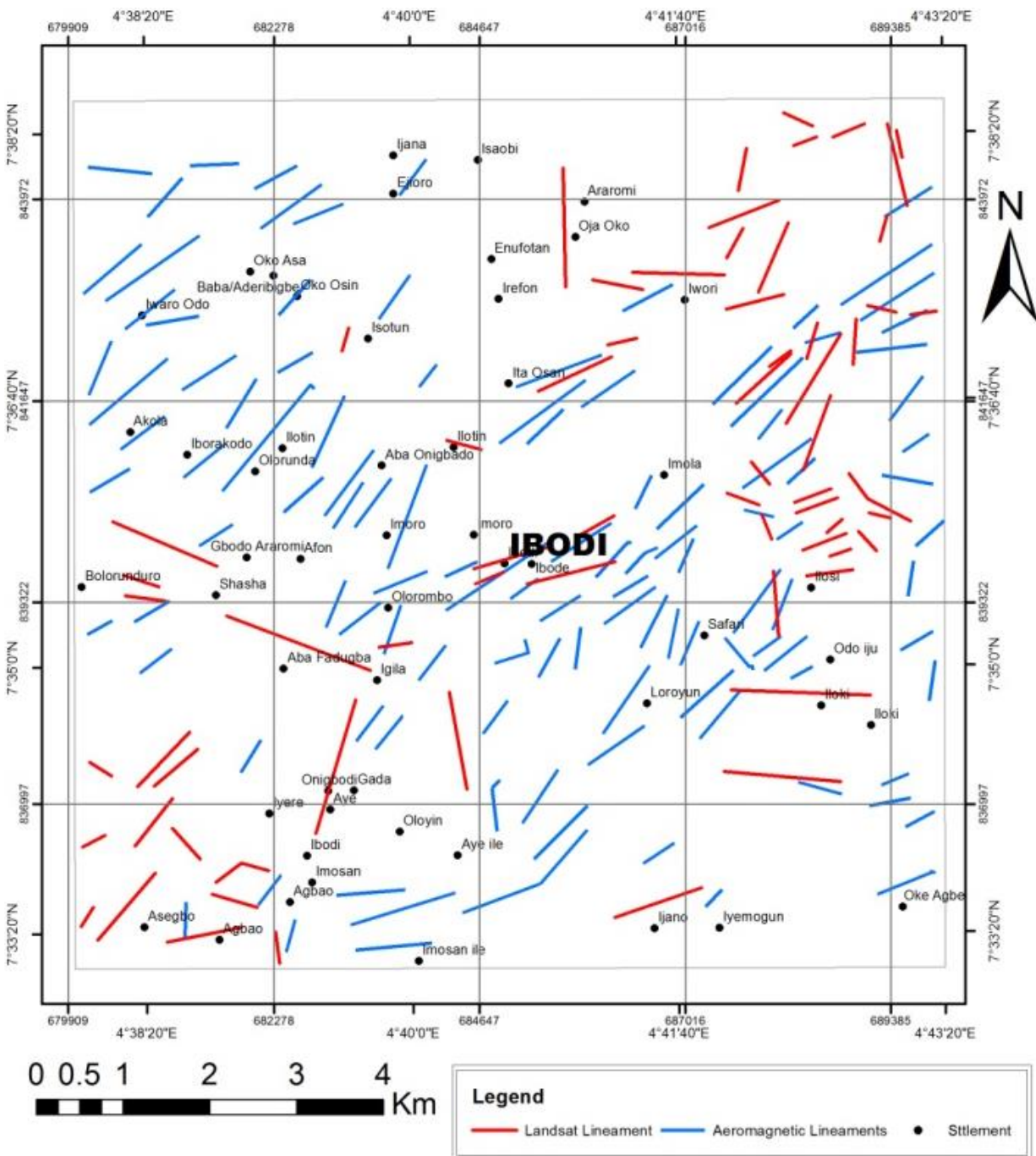


Figure 14. Intersection lineaments map of the study area.

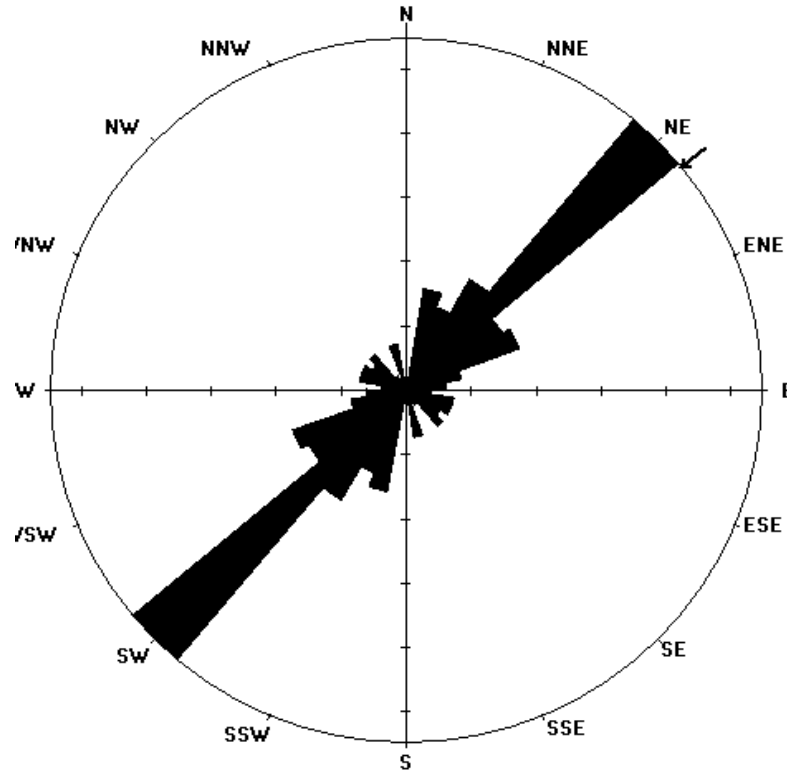


Figure 15. Rose (Azimuth-frequency) diagram of lineament intersections orientations.

more lineament lines. It is obvious from the map that the lineament intersection nodes concentrated within northeastern parts of the study area while other areas are characterized by scanty or no lineaments intersection nodes. The rose (Azimuth-frequency) diagram of the lineaments intersection (Figure 15) was prepared from the extracted lineaments between aeromagnetic and landsat lineaments, which reveals that the lineaments trends mainly NE-SW directions. Here it indicates more fracturing towards the NE direction, suggesting comparatively more potential groundwater zone and hence better prospect for groundwater availability.

Lineaments intersection on topographical and geological map

Figures 16 and 17 display lineament intersection on topographical and geological map. Figure 16 indicates that the lineament intersection nodes concentrated within northeastern part of the study area fall within the plain land while other areas are characterized by scanty or no lineaments intersection nodes. This implies that we cannot base our presumption on surface lineament without ascertain it with subsurface lineaments in order to have clearer pictures of the groundwater prospect within the study area. Figure 17 shows that there are more

lineaments intersection on schist and amphibolites at the northeastern parts followed by gneiss and migmatite undifferentiated while having scanty or low lineaments intersection on amphibolite. This implies that there are more areas with high lineament intersections which are good for groundwater development on schist and amphibolites and gneiss and migmatite undifferentiated while having low lineament intersection on amphibolites, which implies low groundwater development. Regarding groundwater exploration, these aforementioned areas may have high groundwater potentials due to their high concentration of lineament intersections, that is, since groundwater occurs within faults and fractures in the basement rocks.

Superposition of vertical electrical sounding (VES) on lineament intersections

Figure 18 indicates the superposition of vertical electrical sounding (VES) on lineament intersections. Nine VES data were obtained within the investigated area. Figure 19(a to i) shows typical iterated VES data curves and the estimated geoelectric parameters. Four (4) curve types were identified, viz; H, QH, KH and HKH, where curve type KH has the highest occurrences. The curve types were ground on the basis of the aquifer types. The curve

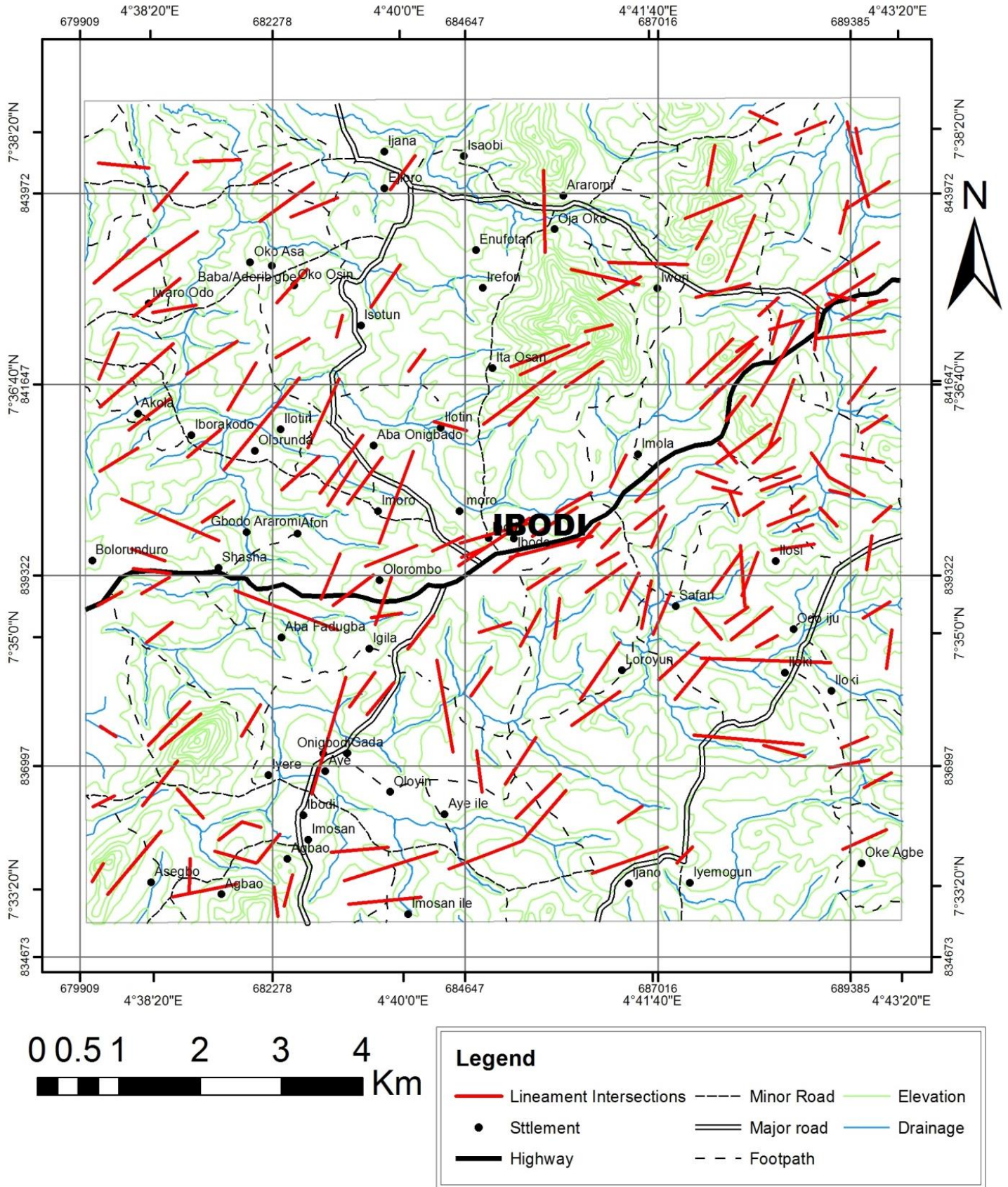


Figure 16. Lineament intersections on topographical map of the investigated area.

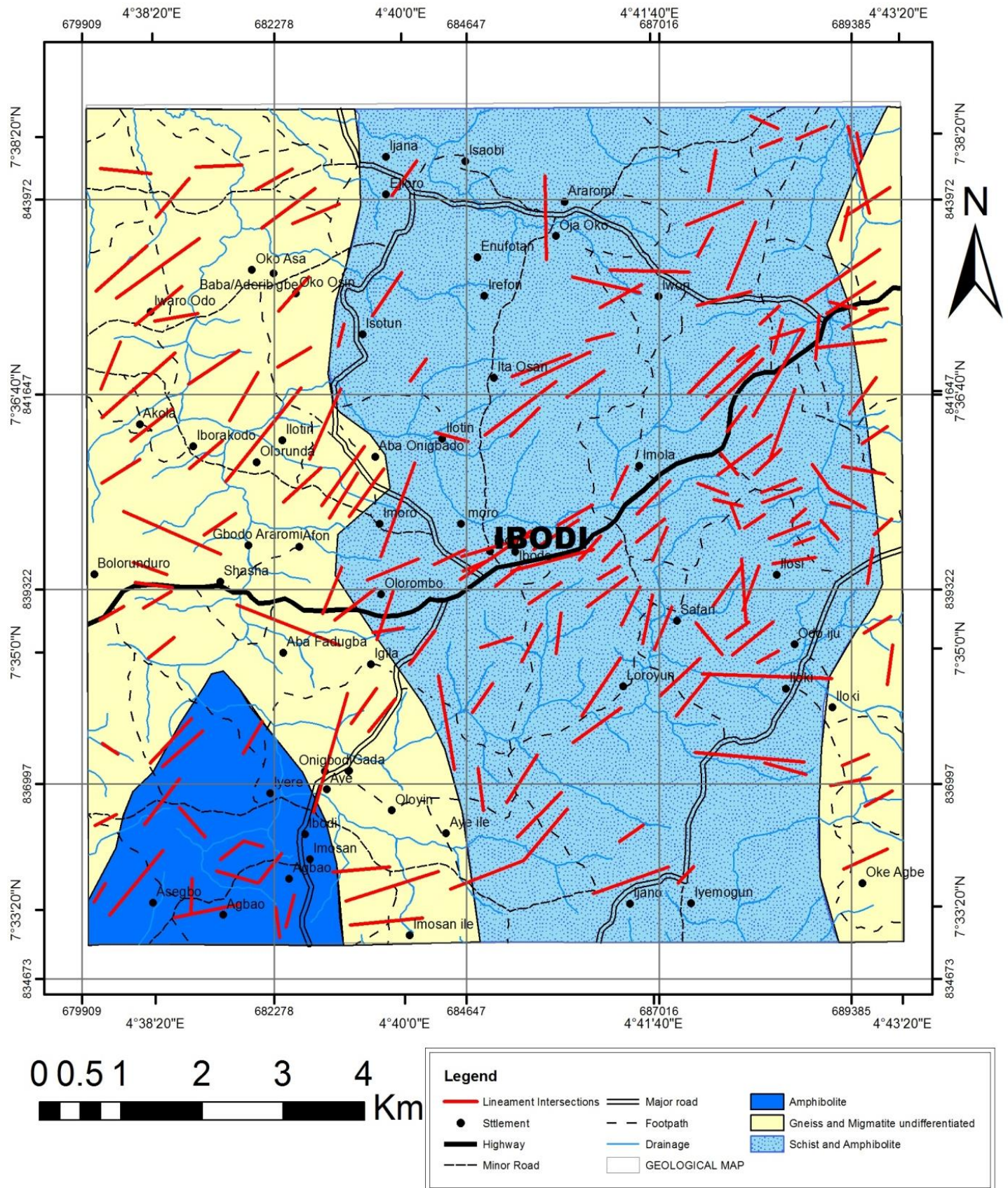


Figure 17. Lineament intersection on geological map of the investigated area.

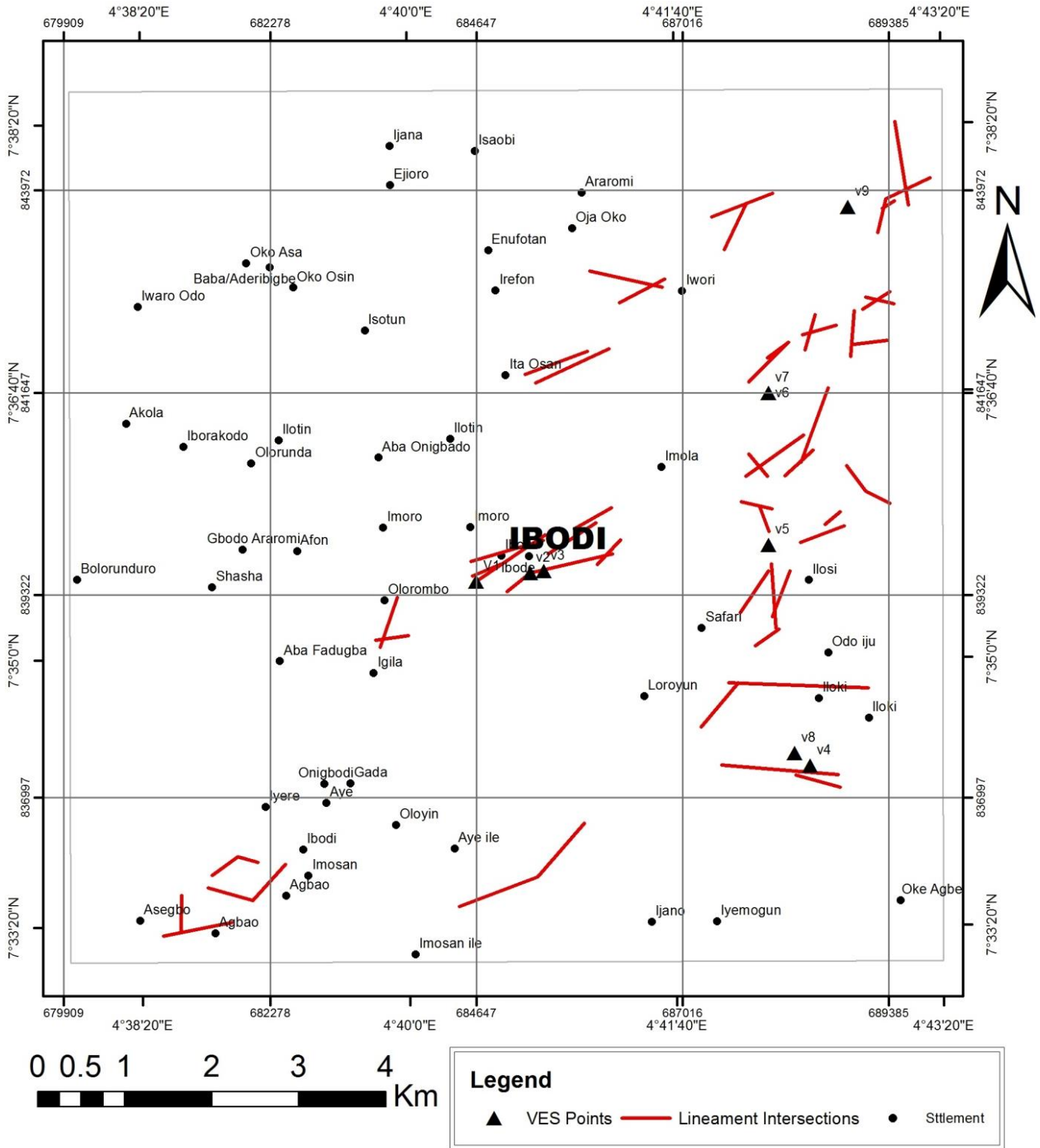
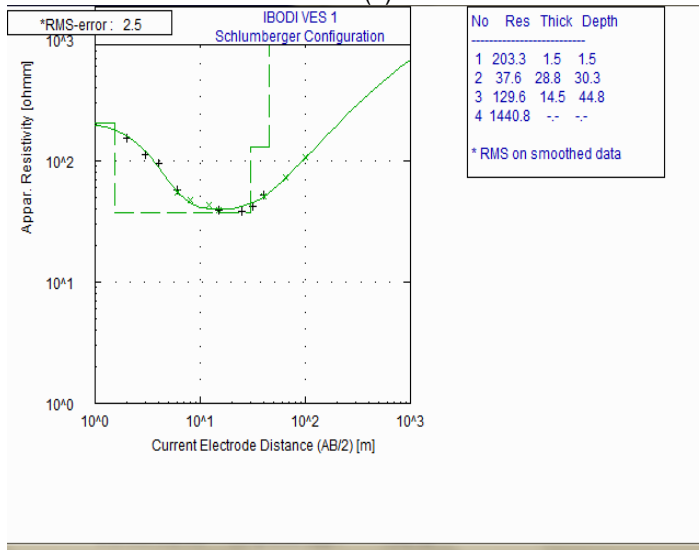


Figure 18. Superposition of vertical electrical sounding (VES) on lineament intersections.

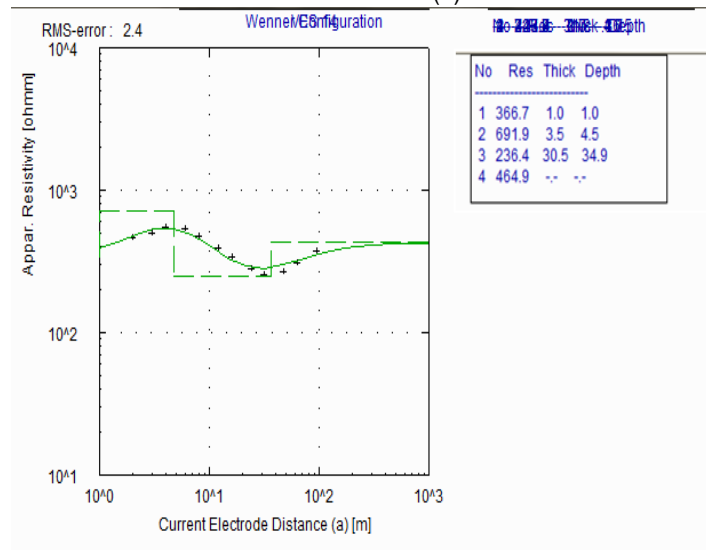
types were ground into three, viz: H and QH, HKH and KH. Aquifer in this group corresponds to layer 2 in H and layer 3 in QH curve types. The aquifer is that of weathered/ partially weathered layer. The groundwater

yield of this type of aquifer is determined by the percentage of clay content. Low groundwater yield is encountered when the aquifer unit is clay. Aquifer in HKH corresponds to the weathered/fractured aquifer

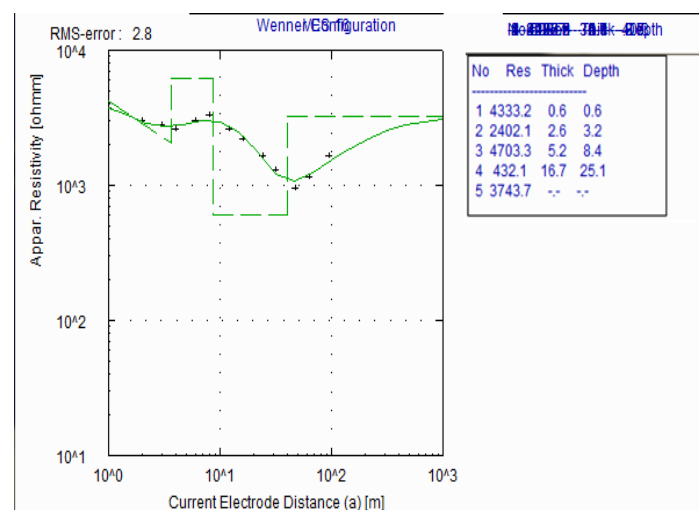
(a) VES 1



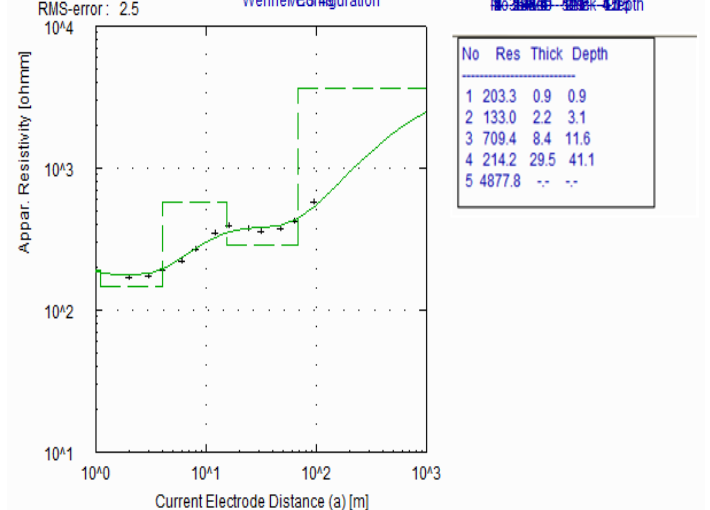
(b) VES 2



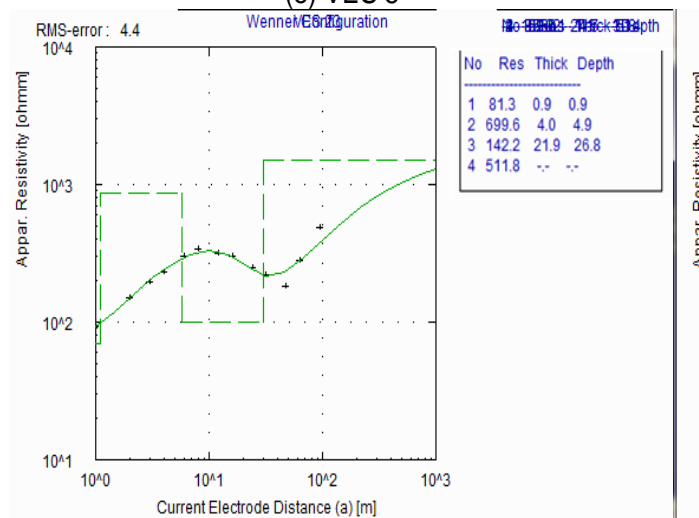
(c) VES 3



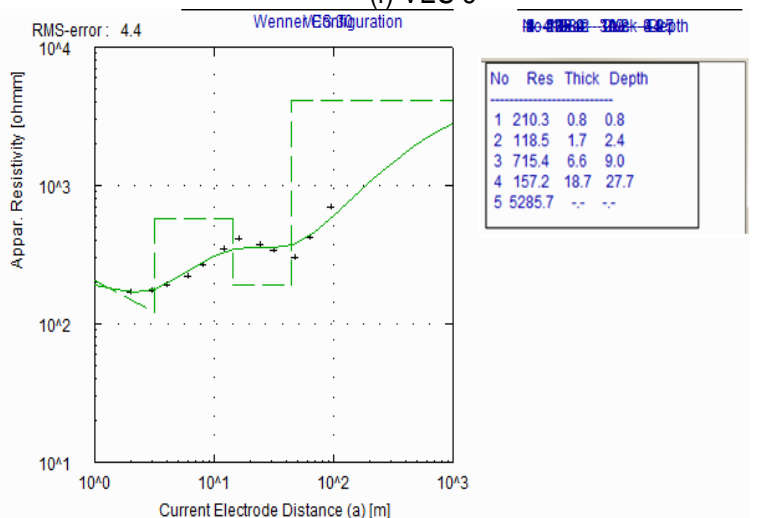
(d) VES 4



(e) VES 5



(f) VES 6



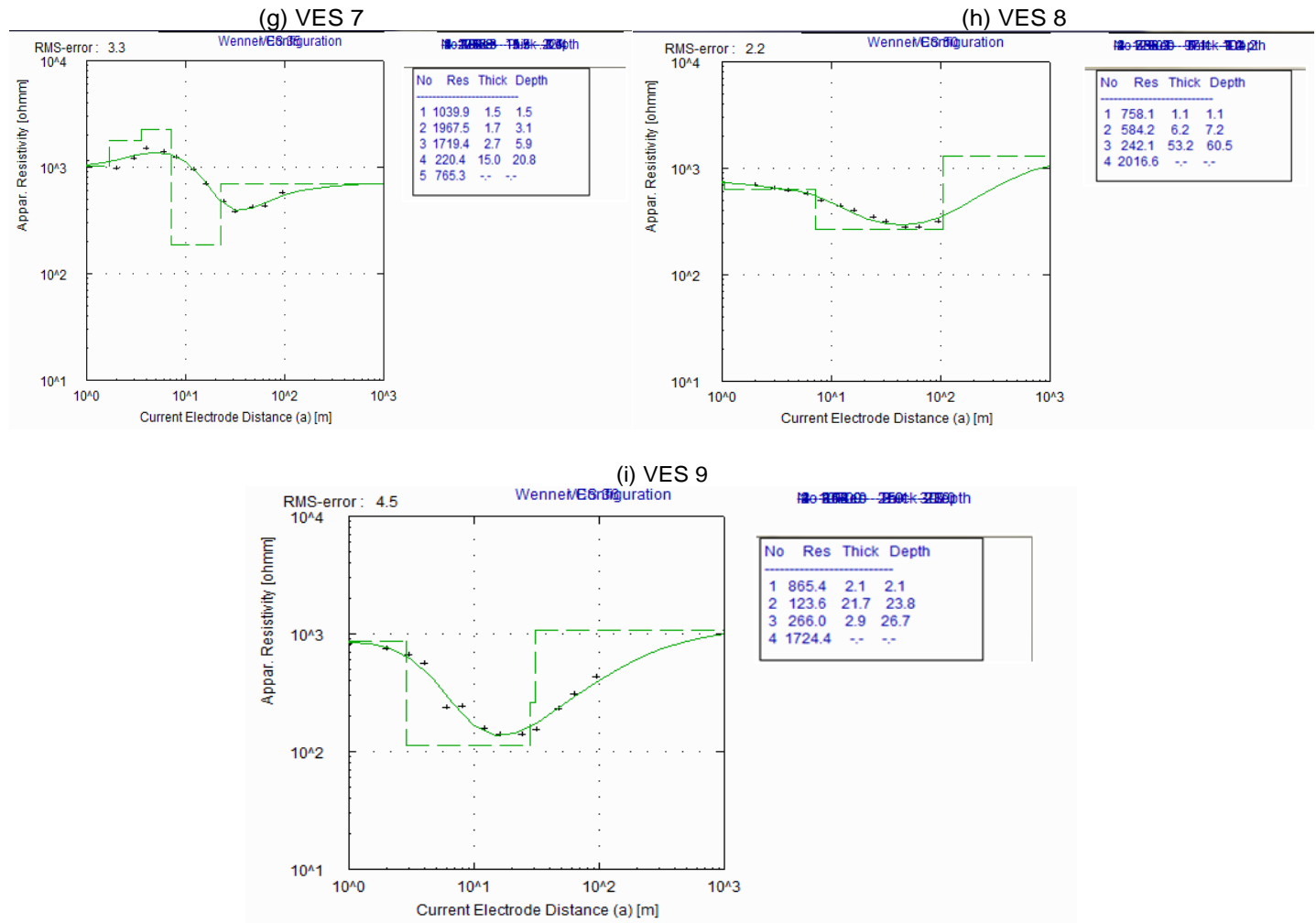


Figure 19. Typical curve types (a) QH (VES 1) (b) KH (VES 2) (c) HKH (VES 3) (d) HKH (VES 4) (e) KH (VES 5) (f) HKH (VES 6) (g) KH (VES 7) (h) KH (VES 8) and (i) QH (VES 9) curves.

(confined). The fractured zone is concealed beneath a fresh basement rock, in which there is no hydraulic communication between the water contains in the weathered layer and the fractured zone, at least within the immediate finite of the abstraction point. Aquifer in KH corresponds to the weathered/fractured (unconfined)/fractured (confined) aquifer. This aquifer types produces very high groundwater yield particularly when the density of the fractures is high. However, area underlain by the weathered/fractured basement aquifer is more promising in terms of groundwater development than the weathered layer aquifer and also the points of intersection in lineament intersections are the point of interest for groundwater development. The VES interpretation results Figure 19a to i of the study area show a total of three to five subsurface layers namely: the topsoil, weathered layer, weathered/fractured basement and fresh basement. The first layer which is the topsoil has resistivity varying from 81 to 4333 Ω m and thickness

ranging from 0.6 to 2.1 m. This layer is relatively thin and with high resistivity. The resistivity of the second layer which is the weathered zone varies from 38 to 700 Ω m while its thickness varies from 1.7 to 28.8 m. The third layer constitutes the weathered/fractured basement which is also being referred to as aquifer layer, and are interpreted as saturated of their relative lower resistivity ranging from 130 to 432 Ω m. The thickness ranges from 2.9 to 52.2 m while the fourth layer is the fresh basement with resistivity values ranging from 455 to 5286 Ω m. The result from the VES data reflects that the areas where the lineament intersected has tendency of very high groundwater prospect. This illustrates that the area will be good for groundwater development.

Lineament intersection density map

Figure 20 exhibit the lineament intersection density map

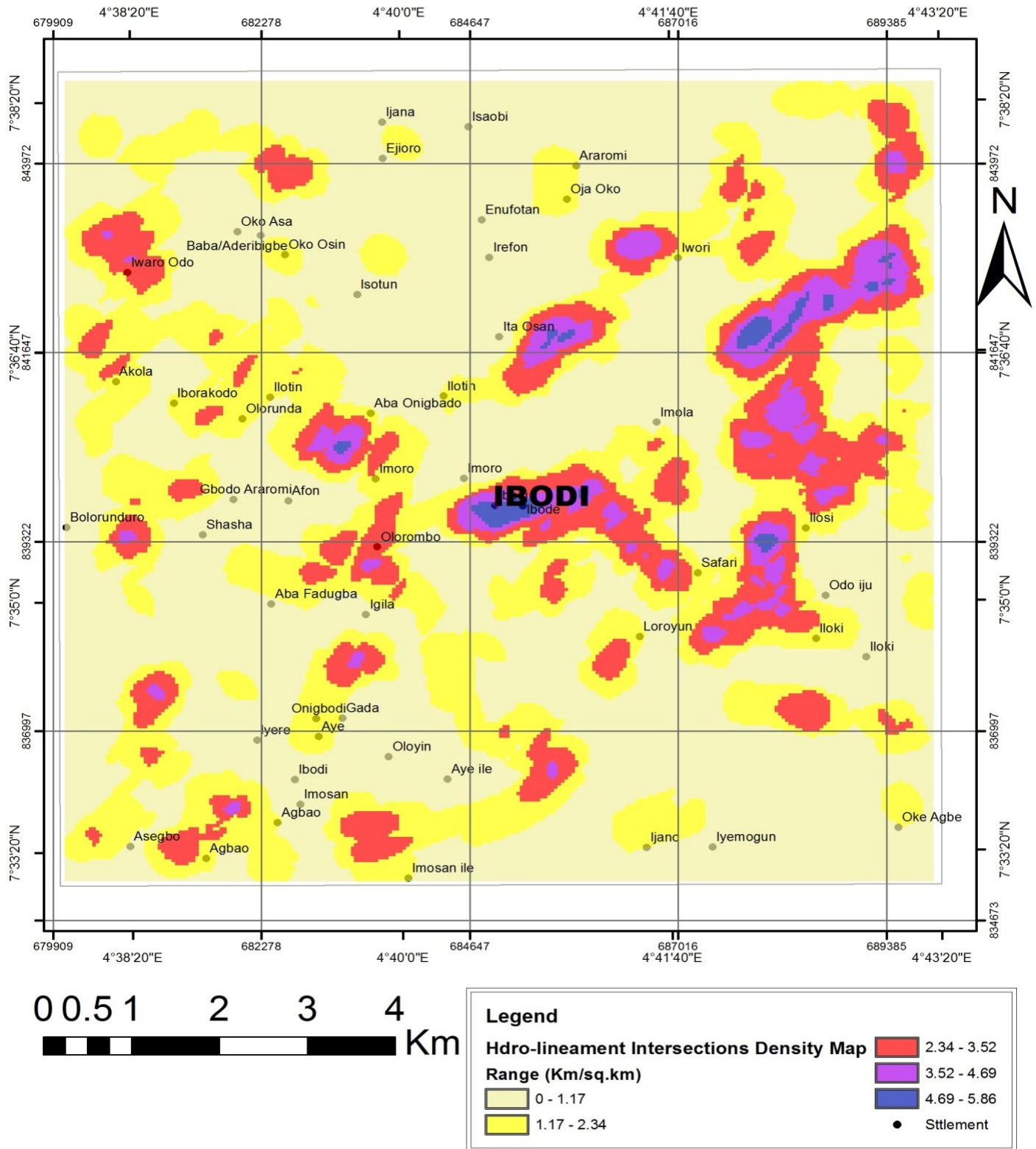


Figure 20. Lineament intersection density map of the study area.

of the study area. Lineament intersection density map is a measure of cluster of linear features in a particular

area. The peaks in the lineament intersection density contour maps are believed to be potential zones for

Table 3. Groundwater prospect of the study area based on lineament intersection density.

Lineaments Density Colour Code	Lineaments Density Range (kg/kg ²)	Groundwater Prospecting
Lemon	0 -1.17	Very Low
Yellow	1.17 - 2.34	Low
Red	2.34 - 3.52	Moderate
Pink	3.52- 4.69	High
Blue	4.69 -5.86	Very High

groundwater resource development. Areas with high lineament intersection density (excluding the residual hill environment) are good for groundwater development (Bayowa et al., 2014). The map revealed five different hydrogeological potential zones distributed as patches in the investigated area. The zones are summarized in Table 3. Considering the groundwater potential classification, it is clear from the lineament intersections density map that area within Ibodi that constitute the central parts of the study area display tendencies for very high groundwater potential. The area appeared on very high lineament intersection zones (areas within Olorombo and Iwaro Odo reflect medium groundwater potential tendencies); on medium lineament intersection zones (areas within Agbao, Oke Agbe, Aye, Onigbodi, Iloki, Sefari, Iwori, Oja Oko, Araromi, Oko Osin, Ilotin, Olorunda and Iborakodo indicate low groundwater potential); and on low lineament intersection zones (areas within Odo Iju, Iyere, Iyemogun, Oloyin, Aye ile, Imosan, Shasha, Enufotan, Ireton, Oko Asa and Ijana show very low groundwater potential tendencies). The localities within these settlements are characterized by very low lineament intersection density.

Conclusions

In this research, groundwater potential of Ibodi and its environs have been investigated using satellite imagery remotely sensed and aeromagnetic dataset. The hydrogeological investigation involved the extraction of lineaments from Landsat Thematic Mapper (TM) satellite imagery and aeromagnetic lineament from the investigated area. The processed image displays the lineaments trending NE-SW directions. Landsat and aeromagnetic lineament trends tend to agree in the study area, implying that these lineaments reflect real continuous fractures at depth. Hydrogeological maps based on lineament and lineament intersections were produced from the generalized lineament trends in the area. The lineament intersection density map identified cluster zones in the range of 0 to 1.17, 1.17 to 2.34, 2.34 to 3.52, 3.52 to 4.69 and 4.69 to 5.86 kg/kg². The map revealed that the concentrations of lineament intersection nodes dominate the eastern and north-eastern parts of the study area while other areas are characterized by

scanty or no lineament intersections nodes. Ibodi falls within the high lineament intersections density zones; however, localities like Olorombo, Iwaro–Odo reflected medium lineament intersection density. Agbao, Oke Agbe, Aye, Onigbodi, Iloki, Sefari, Iwori, Oja Oko and Araromi fall within low lineament intersection density. On the other hand, Odo–Iju, Iyere, Iyemogun, Oloyin, Aye–Ile, Imosan, Shasha and Ijana areas have very low lineament intersection density values. Remote sensing and aeromagnetic dataset has proved to be a useful tool in lineament identification and mapping. The result from the depth sounding data interpretation indicates four curve types which are H, QH, KH and HKH, where curve type KH has the highest occurrence. The results from the vertical electrical sounding data reveal that the areas where the lineament intersected has tendency of very high groundwater prospect. This indicates that the area will be good for groundwater development. The study has led to the delineation of areas where groundwater occurrences are most promising for sustainable supply, suggesting that an area with high concentrations of lineament intersections has a high tendency for groundwater prospecting. This study demonstrates the application of remotely sensed data and aeromagnetic dataset for lineament interpretation in a hard rock hydrogeological environment. The lineament analysis has been effectively done in a GIS environment. The results from the study shows that the remote sensing and aeromagnetic technique is capable of extracting lineament trends in an inaccessible tropical forest.


CONFLICT OF INTERESTS

The authors have not declared any conflict of interests.

REFERENCES

- Amadi AN, Olasehinde PI (2010). Application of Remote Sensing Techniques in Hydrogeological Mapping of Parts of Bosso Area, Minna, North-Central Nigeria. *Int. J. Phys. Sci.* 5:1465-1474.
- Amudu GK, Onwuemesi AG, Ajaegwu NE, Onuba LN, Omali AO (2008). Electrical resistivity investigation for groundwater in the Basement Complex terrain: a case study of Idi-Ayunre and its environs, Oyo State, Southwestern Nigeria. *Nat. Appl. Sci. J.* 9(2):1-12.
- Banks D, Odling NE, Skarphagen H, Rohr-Torp E (1996). Permeability and stress in crystalline rocks. *Terra Nova* 8:223-235.

- Bayowa OG, Olorunfemi MO, Akinluyi FO, Ademilua OL (2014). Integration of Hydrogeophysical and Remote Sensing data in the assessment of groundwater potential of the basement complex terrain of ekiti state, southwestern Nigeria. *Ife J. Sci.* 16(3).
- Caine JS, Evans JP, Forster CB (1996). Fault zone architecture and permeability structure. *Geology* 24:1025-1028.
- Evans JP, Forster CB, Goddard JV (1997). Permeability of fault-related rocks and implications for hydraulic structure of fault zones. *J. Struct. Geol.* 19:1393-1404.
- Hardcastle KC (1995). Photolineament factor: A new computer-aided method for remotely sensed fractured. *Photogrammetric Eng. Rem. Sens.* 61(6):739-747.
- Henriksen H, Braathen A (2006). Effects of fracture-lineaments and in situ rock stresses on groundwater flow in hard rock. A case study from Sunnfjord, Western Norway. *Hydrogeol. J.* 14:444-461.
- Hobbs WH (1904). Lineaments of the Atlantic border region. *Geol. Soc. Am. Bull.* 15:483-506.
- Hobbs WH (1912). *Earth Features and Their Meaning: An Introduction to Geology for the Student and General Reader.* Macmillan Co. New York. 347.
- Hung LQ, Batelaan O, De Smedt F (2005). Lineament extraction and analysis, comparison of Landsat ETM and Aster imagery. Case study: Suoimuoi tropical karst catchment, Vietnam. *Proc. SPIE* 5983(5983):1-12.
- Montaj TM Tutorial (2004). Two – Dimension frequency domain processing of potential field data. 1-67 Toronto, Canada, Geosoft Incorporated: 2-90.
- Leary O, Freidman DW, Pohn JD (1976). Lineaments, linear, lineation- some proposed new standards for old terms. *Geol. Soc. Am. Bull.* 87:1463-1469.
- Olade MA (1978). General features of a Precambrian iron deposit and its environment at Itakpe Ridge Okene, Nigeria. *Trans. Inst. Min. Metallurgy Sect.* 87:81-89.
- Olorunfemi MO, Fasuyi SA (1993). Aquifer Types and the Geoelectric/Hydrogeologic Characteristics of Part of the Central Basement Terrain of Nigeria (Niger State). *J. Afr. Earth Sci.* 16:309-317.
- Osun State Ministry of Lands and Physical Planning (1965). Topographical Map of Ilesha southwestern Sheet 234.
- Osun State Ministry of Lands and Physical Planning (1980). Geological Map of Ilesha Iwo Sheet 60.
- Rahaman MA (1976). Review of the basement of S.W. Nigeria. In: Kogbe (ed) *Geology of Nigeria.* Elizabethan press, Lagos. pp. 41-58.
- Zohdy AAR, Martin RJ (1993). A study of sea water intrusion using direct current sounding in the Southern part of the Ox ward Plain California. Open-file reports 93 – 524 U. S. Geological Survey. 13.



International Journal of Physical Sciences

Related Journals Published by Academic Journals

- *African Journal of Pure and Applied Chemistry*
- *Journal of Internet and Information Systems*
- *Journal of Geology and Mining Research*
- *Journal of Oceanography and Marine Science*
- *Journal of Environmental Chemistry and Ecotoxicology*
- *Journal of Petroleum Technology and Alternative Fuels*

academicJournals